

# Enhancing disaster risk resilience using greenspace in urbanising Quito, Ecuador

C. Scott Watson<sup>1</sup>, John R. Elliott<sup>1</sup>, Susanna K. Ebmeier<sup>1</sup>, María Antonieta Vásquez<sup>2</sup>, Camilo Zapata<sup>2</sup>, Santiago Bonilla-Bedoya<sup>3</sup>, Paulina Cubillo<sup>4</sup>, Diego Francisco Orbe<sup>4</sup>, Marco Córdova<sup>5</sup>, Jonathan Menoscal<sup>5</sup>, Elisa Sevilla<sup>2</sup>

<sup>1</sup>COMET, School of Earth and Environment, University of Leeds, Leeds, LS2 9JT, UK.

<sup>2</sup>College of Social Sciences and Humanities, Universidad San Francisco de Quito, Quito 170901, Ecuador.

<sup>3</sup>Research Center for the Territory and Sustainable Habitat, Universidad Tecnológica Indoamérica, Machala y Sabanilla, 170301, Quito, Ecuador.

<sup>4</sup>Centro de Información Urbana de Quito - CIUQ, Quito, Ecuador.

<sup>5</sup>Facultad Latinoamericana de Ciencias Sociales - Flacso, Quito, Ecuador.

*Correspondence to:* C. Scott Watson (c.s.watson@leeds.ac.uk)

## Abstract

Greenspaces within broader ecosystem-based disaster risk reduction strategies (Eco-DRR) provide multiple benefits to society, biodiversity, and addressing climate breakdown. In this study, we investigated urban growth, its intersection with hazards, and the availability of greenspace for disaster risk reduction (DRR) in the city of Quito, Ecuador, which experiences multiple hazards including landslides, floods, volcanoes, and earthquakes. We used satellite data to quantify urban sprawl and developed a workflow incorporating high resolution digital elevation models (DEMs) to identify potential greenspaces for emergency refuge accommodation (DRR greenspace), for example following an earthquake. Quito's historical urban growth totalled ~192 km<sup>2</sup> 1986–2020 and was primarily on flatter land, in some cases crossed by steep ravines. By contrast, future projections indicate an increasing intersection between easterly urbanisation and steep areas of high landslide susceptibility. Therefore, a timely opportunity exists for future risk-informed planning. Our workflow identified 18.6 km<sup>2</sup> of DRR greenspaces, of which 16.3 km<sup>2</sup> intersected with potential sources of landslide and flood hazards, indicating that hazard events could impact potential 'safe spaces'. These spaces could mitigate future risk if designated as greenspaces and left undeveloped. DRR greenspace overlapped 7% (2.5 km<sup>2</sup>) with municipality designated greenspace. Similarly, 10% (1.7 km<sup>2</sup>) of municipality designated 'safe space' for use following an earthquake was classified as potentially DRR suitable in our analysis. For emergency refuge, currently designated greenspaces could accommodate ~2–14% (depending on space requirements) of Quito's population within 800 m. This increases to 8–40% considering all the potential DRR greenspace

31 mapped in this study. Therefore, a gap exists between the provision of DRR and designated greenspace. Within Quito, we  
32 found a disparity between access to greenspaces across socio-economic groups with lower income groups having less access  
33 and further to travel to designated greenspaces. Notably, the accessibility of greenspaces was high overall with 98% (2.3  
34 million) of Quito's population within 800 m of a designated greenspace, of which 88% (2.1 million) had access to potential  
35 DRR greenspaces. Our workflow demonstrates a citywide evaluation of DRR greenspace potential and provides the  
36 foundation upon which to evaluate these spaces with local stakeholders. Promoting equitable access to greenspaces,  
37 communicating their multiple benefits, and considering their use to restrict propagating development into hazardous areas  
38 are key themes that emerge for further investigation.

## 39 **1 Introduction**

40 Urbanising and increasing populations are a global trend that create a range of societal and environmental challenges  
41 including food and water security (Godfray et al., 2010; Hoekstra et al., 2018), air pollution (Fenger, 1999; Escobedo and  
42 Nowak, 2009; Zalakeviciute et al., 2018), disease (Marmot et al., 2008), loss of biodiversity (McDonald et al., 2020), climate  
43 change (De Sherbinin et al., 2007; Flörke et al., 2018), and exposure to disaster risk (Pelling et al., 2004). Approximately  
44 68% of the world's population are projected to live in urban areas by 2050, many of which are yet to be developed, and the  
45 rate of urbanisation is greatest for developing countries (UN DESA, 2019). Development of informal settlements takes place  
46 outside of regulatory frameworks such as land use planning or building design codes (UN-Habitat, 2003; Oliver-Smith et al.,  
47 2016). Therefore, urbanisation often occurs within or creates hazardous areas, which exacerbates the socioeconomic  
48 inequalities of disaster risk due to overcrowding, unsafe housing, and lack of infrastructure and services (Baker, 2012;  
49 Cardona et al., 2012). Reducing disaster risk and losses is the aim of the global Sendai Framework for Disaster Risk  
50 Reduction 2015–2030 (UNDRR, 2015) and is integral to achieving the UN sustainable development goals (SDGs).  
51 Specifically, Goal 11 to 'make cities and human settlements inclusive, safe, resilient and sustainable' targets reducing deaths  
52 and socio-economic impacts associated with disasters with a focus on the most vulnerable (UN General Assembly, 2015).  
53 Successful risk reduction in 'tomorrow's cities' requires people-centred decision making to support a transition from disaster  
54 response to risk-informed planning (Galasso et al., 2021). Additionally, nature-based solutions (NbS) involving greenspace  
55 in cities are increasingly recognised within a framework of Ecosystem-based Disaster Risk Reduction (Eco-DRR) (Estrella  
56 and Saalismaa, 2013; Faivre et al., 2018; UNDRR, 2020) and can be designed and monitored using an increasing number of  
57 earth observation (EO) technologies (Kumar et al., 2021). EO data are widely used for land cover classifications to quantify  
58 historical trends in urban expansion and to model future urbanisation projections (Schneider and Woodcock, 2008; Bonilla-  
59 Bedoya et al., 2020b). Both high-resolution (< 1 m, commercial) (Myint et al., 2011; Georganos et al., 2018) and medium  
60 resolution (10–30 m, open-access) (e.g. Landsat and Sentinel-2) optical satellite imagery are used for land cover and  
61 greenspace mapping (Fuller et al., 1994; Labib and Harris, 2018; Deng et al., 2019).

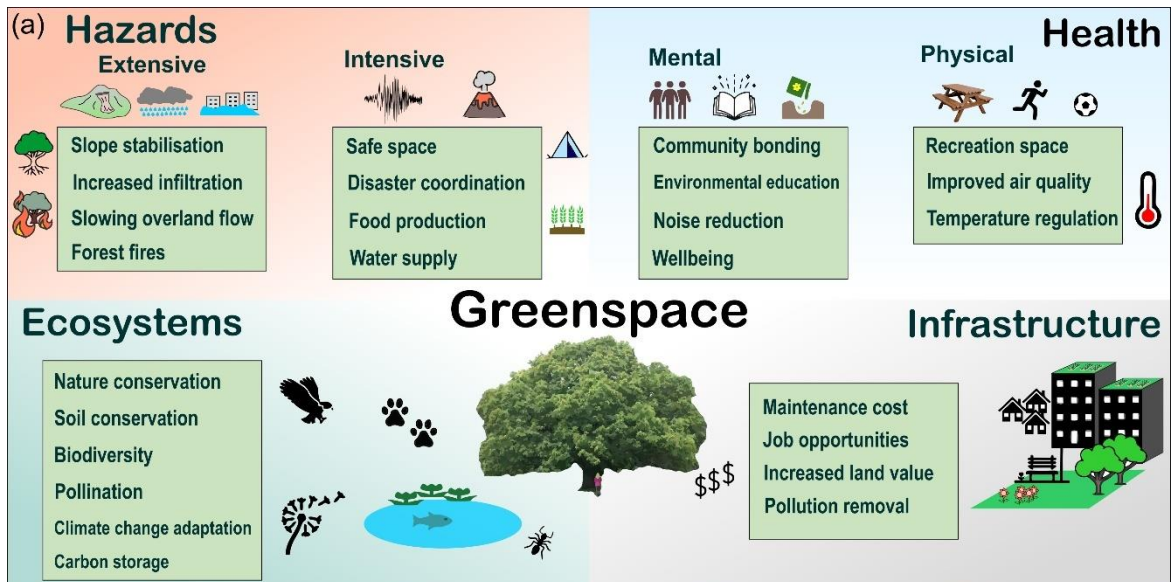
62

63 There are multiple definitions of greenspace, however, they generally include reference to public parks, gardens, open space,  
64 wetlands, street verges, woodland, and sports grounds (Taylor and Hochuli, 2017). Greenspace is associated with multiple  
65 impacts on urban and natural systems (Fig. 1a) including: improving mental and physical health (James et al., 2015; WHO  
66 Regional Office for Europe, 2016; Marselle et al., 2020; Bauwelinck et al., 2021); conserving natural ecosystems and  
67 biodiversity (Aronson et al., 2017; McDonald et al., 2020); creating economic opportunities (Gregory McPherson, 1992);  
68 building community resilience to hazards (Colding and Barthel, 2013), including reducing landslide risk (Phillips and  
69 Marden, 2005; Sandholz et al., 2018) and urban flooding (Maragno et al., 2018); and providing safe spaces in the event of a  
70 disaster (Shrestha et al., 2018; Sphere Association, 2018; Shimpo et al., 2019; Jeong et al., 2021). However, greenspace  
71 planning in urban environments is often recreation focused (Boulton et al., 2018). Therefore, it is important to recognise the  
72 provision of multi-benefit greenspaces within an Eco-DRR framework, and the diverse accessibility, ownership, and  
73 management of such spaces (Colding and Barthel, 2013). Similarly, the creation and designation of greenspace requires  
74 consideration of social justice issues, such as the impact on property values (Wolch et al., 2014; García-Lamarca et al.,  
75 2020).

76  
77 Green cities, which incorporate diverse greenspace, green infrastructure, and interconnected social and ecological networks,  
78 provide opportunities to enhance disaster resilience and deliver multiple benefits for sustainable development and nature  
79 conservation (Benedict and MacMahon, 2002; Tidball and Krasny, 2012). These elements may be designed and integrated  
80 into planning policy (Jeong et al., 2021) or emerge following crises, such as loss of food security prompting the proliferation  
81 of urban gardening (Altieri et al., 1999; Gonzalez, 2003; Colding and Barthel, 2013). Similarly, following disaster events  
82 such as earthquakes, open spaces are used for emergency refuge (Allan et al., 2013; Borland, 2020). The latter point was the  
83 case following the 2015 Gorkha earthquake in Nepal, where greenspaces were used for temporary accommodation away  
84 from collapsed and damaged buildings (Fig. 1 b-c). Temporary government camps homed over 30,000 people in the  
85 Kathmandu Valley and over 1,000 smaller shelter sites homed thousands more (Khazai et al., 2015). Greenspace was also  
86 prioritised in Tokyo following the 1923 Great Kantō Earthquake, where parks originally designed to provide space for  
87 children were later valued as emergency refuges (Borland, 2020). Innovative greenspace design elements may also emerge  
88 following disaster events, such as integrating water bodies and pumps, edible plant species, and multi-purpose (e.g. seating,  
89 dining, and cooking) communal seating areas into greenspace areas (Bryant and Allan, 2013).

90  
91 Historically, green space in Quito was defined by the rural-urban relationship. Until the end of the 19th century, green spaces  
92 were the "Ejidos", sites for agriculture and livestock, which were located on the outskirts of the city. The urbanisation model  
93 did not contemplate green spaces in its design and natural spaces such as the ravines were mostly filled in (Aragundi et al.,  
94 2016). This is important because parks and plazas have been repeatedly used as refuge sites after earthquakes in Quito. For  
95 example, during the 1859 Quito earthquake and 1868 Ibarra earthquake, refugee tents were set in the main plazas and parks

96 of the city (e.g. Figure 1d, e). During the 20th Century, the use of these greenspaces and open spaces like plazas as refuge  
97 after earthquakes was recognised through the creation of official 'safe spaces' (see section 4.3) (Metro Ecuador, 2019).



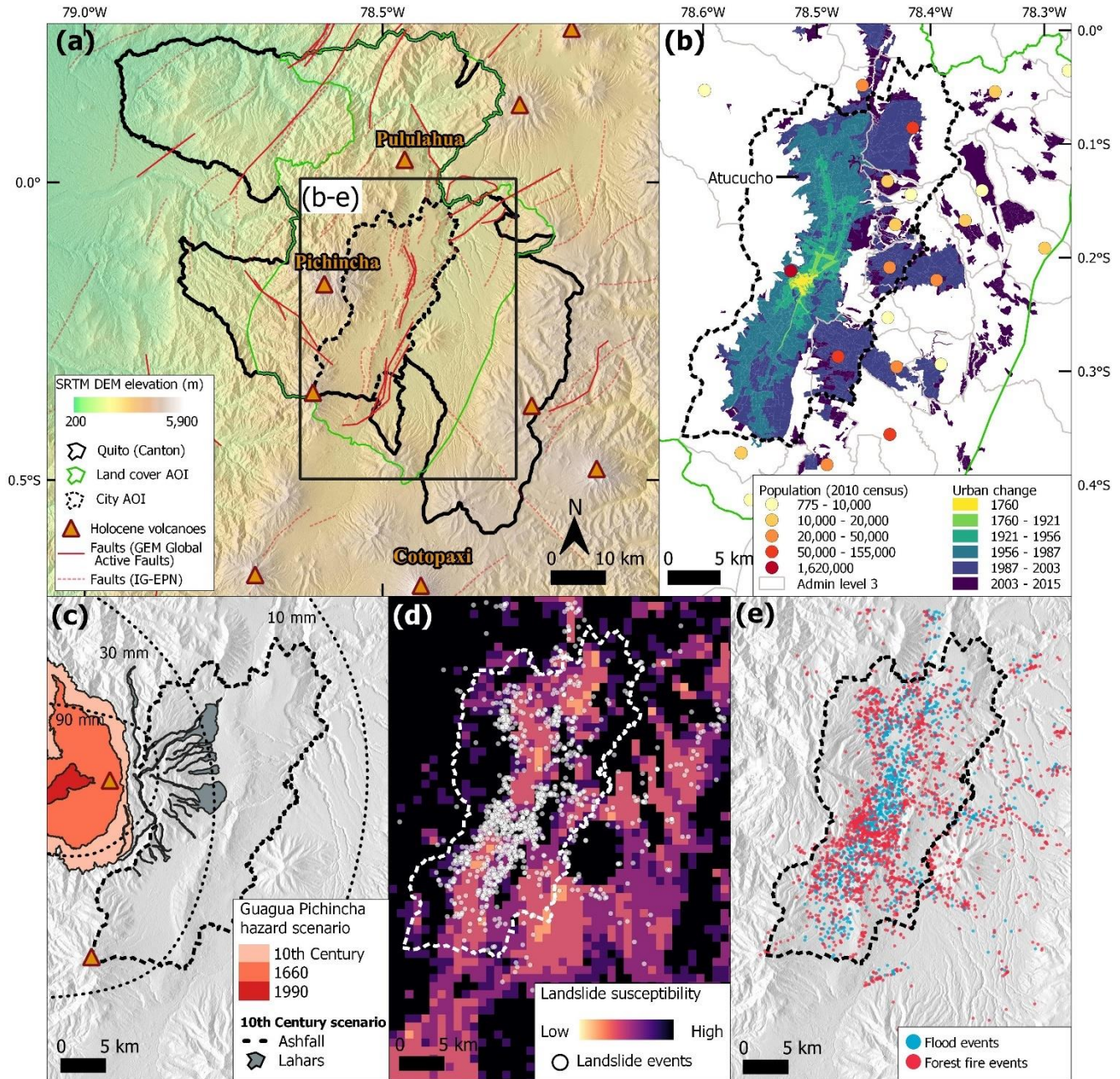
99 **Figure 1: (a) Example impacts of urban greenspace on hazards, health, ecosystems, and infrastructure. (b-c) An area of**  
100 **greenspace ‘Tundikhel’ (Lat: 27.702°, Lon: 85.315°) in Kathmandu, Nepal, which was used for temporary tented accommodation**  
101 **following the Gorkha earthquake (25 April 2015). (d-e) Tents in Plaza Santo Domingo and Plaza Mayor (Plaza Grande) in Quito**  
102 **after the 1868 Ibarra earthquake.**

103  
104 Quito has a population of over 2 million (2020), having doubled in just three decades from 1 million in the late 1980s, and  
105 which is projected to exceed 3.4 million by 2040 (DMQ, 2018). The expansion of formal and informal settlements into  
106 hazardous areas increases disaster risk from events including landslides, flooding, volcanic eruptions, and earthquakes.  
107 Increased disaster risk is due to both increased exposure to natural hazards and the social vulnerability of the exposed  
108 communities (e.g. Valcárcel et al., 2017). Therefore, in this study we assessed the potential of greenspace for reducing  
109 disaster risk in contemporary Quito, and for guiding the development of more resilient communities in future urban areas.  
110 Specifically, we: (1) quantified Quito’s recent historical urban expansion using satellite-based optical imagery and evaluated  
111 potential future urbanisation scenarios using land classification metrics; (2) investigated the intersection between the built  
112 environment and natural hazards; and (3) evaluated the potential role of urban greenspace for reducing disaster risk in Quito  
113 by providing ‘safe spaces’. In this study, we analyse a style of greenspace relevant to disaster risk reduction that is  
114 quantifiable using optical satellite data. Specifically, we focus on low gradient open spaces that are vegetated. We do not  
115 consider specific greenspace amenities such as recreation facilities, or accessibility restrictions, which cannot be determined  
116 using satellite data alone.

## 117 **2 Study region**

118 Quito is situated in the central region of Ecuador, just south of the equator in the Inter-Andean Valley of South America at  
119 over 2,800 m a.s.l. and is bounded by Pichincha Volcano (4794 m) to the west and steep topography to the east (Fig. 2).  
120 Topography and factors such as the intertropical convergence zone and the South Atlantic convergence zone determine  
121 Quito’s climate (Hastenrath, 1997; Vincenti et al., 2012; Zambrano-Barragán et al., 2011). Quito’s precipitation distribution  
122 has two modalities, March–April and October–December, with an average annual precipitation of 1200 mm and an average  
123 annual temperature of 13.4°C (Vincenti et al., 2012; Zambrano-Barragán et al., 2011). In recent decades, Quito’s urban  
124 extent has spread many kilometres to the north, east, and south (Bonilla-Bedoya et al., 2020b; Salazar et al., 2020).  
125 Westward expansion is limited, although not absent, due to the designated protected areas on the slopes of Pichincha  
126 volcano, which were implemented following urban encroachment and the incidence of landslides and floods (Vidal et al.,  
127 2015; DMQ, 2018). Urban expansion is changing Quito’s exposure to natural hazards including landslides, floods, volcanic  
128 activity, and earthquakes (Chatelain et al., 1999; Hall et al., 2008; Carmin and Anguelovski, 2009; Valcárcel et al., 2017).  
129 Quito’s urban area now exceeds the current Metropolitan District of Quito (DMQ) administrative boundary (Bonilla-Bedoya  
130 et al., 2020a; Salazar et al., 2021). Therefore, in this study, we define two separate areas of interest (AOIs): (1) a ‘land cover  
131 AOI’ for mapping land cover change, which encompasses the core urban area of Quito, and (2) a ‘city AOI’ for mapping

132 greenspace, which includes the Administrative Level 3 Parishes of Quito, Cumbaya, Llano Chico, Calderon (Carapungo),  
 133 Conocoto, Zambiza, and Nayón (Fig. 2a, S1).



134  
 135 **Figure 2: (a) The location of Quito, Ecuador in relation to regional seismic faults and volcanoes. Fault lines (red) are from the**  
 136 **Geophysical Institute of the National Polytechnic School (IG-EPN) and Global Earthquake Model Global Active Faults (Styron,**  
 137 **2019). (b) Urban change and population of Quito are mapped using Open Government data (<http://gobiernoabierto.QUITO.gob.ec/>).**  
 138 **(c) Volcanic hazards from the IG-EPN et al. (2019) Pichincha Volcano hazard map. (d) Landslide susceptibility map (Stanley and**

139 **Kirschbaum, 2017) and observed landslide events (n=1,321) (2006–2017) (<http://gobiernoabierto.quito.gob.ec/>).** (e) **Observed**  
140 **Hydrometeorological (n=1,574) and forest fire events (n=2,358) (2006–2017) (<http://gobiernoabierto.quito.gob.ec/>).**

141

142 Quito is surrounded by active faults (Fig. 2a) and the Global Earthquake Model estimates (Pagani et al., 2018) at the regional  
143 scale indicate a relatively high seismic hazard with a Peak Ground Acceleration (PGA) of 0.55–0.9 g (with a 10%  
144 probability of exceedance in 50 years) (Fig. S1). Similarly, Beauval (2018) estimate a PGA of ~0.4–0.6 g for Quito in a  
145 return period of 475 years. The Quito Fault System creates seismic hazard across the city, with a maximum earthquake size  
146 estimated at  $M_w$  6.6 and a recurrence time of ~150–435 years (Alvarado et al., 2014). Earthquake scenario damage models  
147 show that the highest rates of potential building damage are associated with areas of highest social vulnerability (Valcárcel et  
148 al., 2017). Volcanic eruptions also pose significant risk to large populations. Quito lies 12 km from the active volcano  
149 Guagua Pichincha, where activity over the past decades has been characterised by small explosions, ash, and gas emission  
150 (Loughlin et al., 2015). Past eruptions have covered Quito in ash, for example, the 1660 eruption ash deposits are ~10 cm  
151 thick in central Quito (Robin et al., 2008). Recent pyroclastic flows and surges have been channelled by topography away  
152 from Quito to the west, but potential volcanic hazards in Quito include secondary lahars as well as ashfall, which are mapped  
153 using knowledge of historic eruptions (IG-EPN, 2019) (Fig. 2c). Quito’s road network, and water supply, are also all  
154 vulnerable to flows and especially ash from multiple volcanoes (Wilson et al., 2012; Loughlin et al., 2015). Landslides and  
155 floods are both extensive natural hazards in Quito owing to the steep topography, intense rainfall, and filling of natural  
156 drainage channels to create building space (DMQ, 2018; Castelo et al., 2018; Domínguez-Castro et al., 2018; Perrin et al.,  
157 2001). Landslides are concentrated on the steep slopes of Quito’s periphery and ravines (Fig. 2d), whereas flood events are  
158 spread across Quito’s urban extent (Fig. 2e). Following heavy rainfall, mudflows are also a hazard on the lower and  
159 increasingly urbanised slopes of Pichincha (Perrin et al., 2001). Multi-hazards or cascading hazards could also emerge  
160 through combinations of single hazards, such as a volcanic eruption that deposits ash on slopes and blocks urban drains,  
161 which if followed by heavy rain could produce lahars and urban flooding respectively (Gill et al., 2021).

162

163 In terms of policy and planning, the issue of green space in the city currently maintains a spatial-functional emphasis,  
164 although environmental (mainly related to climate change) and socio-political (public space, right to the city) criteria have  
165 been incorporated. There was an important change in the first urban plan of the city (1942), where the design envisages a  
166 series of green spaces, especially in the north of the city, under a criterion of recreational and sports spaces. This is the case  
167 of the current La Carolina park, which was initially the city's racecourse. The plan also considered a series of smaller green  
168 spaces within the residential areas. However, a balanced development between urban sprawl and the environment was not  
169 planned, but rather green and open spaces in general were thought of as part of the zoning logic of the time. This model of  
170 urban development between the 1970s and 2000s is the main risk factor for disasters in the city (Carrión and Erazo Espinosa,  
171 2012). In 1993, the Metropolitan District of Quito (DMQ) was created, with 9.3% of its territory being urban and 90.7%



172 rural. This new territorial configuration is relevant because both planning and risk analysis tend to concentrate only on the  
173 urbanised area (Peralta Arias and Higuera García, 2016).

174

175 When outlining the vision of Quito to year 2040, the Municipality of the Metropolitan District of Quito recognised the  
176 importance of an urban green network for delivering social and natural benefits, including risk mitigation (DMQ, 2018). This  
177 recognition of greenspace to reduce risk from morphoclimatic events has been present in the planning instruments of the  
178 Municipality since the 1980s. The destructive mudflows of 1983 on the slopes of Pichincha that had been previously  
179 urbanised by informal settlements prompted the national government of Ecuador to legislate for the law on “protective  
180 forests”. These forests were designed to prevent erosion, mitigate landslides, and control informal urbanisation on slopes  
181 around Quito. According to Sierra (2009), the role of greenspace in the borders of the city were first designed as recreational  
182 and patrimonial landscapes from 1940s onwards, and later, in the 1970s and 1980s incorporated environmental, city growth  
183 control, and risk mitigation properties. In the last 30 years, there has been Municipal and community interest in the recovery  
184 of ravines for recreational activities and improving citizens quality of life by implementing nature-based solutions alongside  
185 urban development; however, its realisation and impact has been small at the city scale, instead confined to planning-stage  
186 pilot projects such as in the San Enrique de Velasco district in the northwest of Quito (Salmon et al., 2021).

187

188 The following section details our methodology to quantify Quito’s historical urban growth and investigation of future urban  
189 growth scenarios. We investigate Quito’s growth in conjunction with topographical information and hazard datasets to reveal  
190 how Quito’s exposure to hazards is changing through time. We then define a methodology to map greenspace that is  
191 potentially suitable for disaster risk reduction, considering the spatial distribution in relation to socioeconomic data, and per  
192 person accessibility if the spaces were used as an emergency refuge. These data are then used to reveal optimum locations  
193 for the designation of new protected greenspaces to enhance disaster risk resilience in Quito.

## 194 **3 Methodology**

### 195 **3.1 Urban growth**

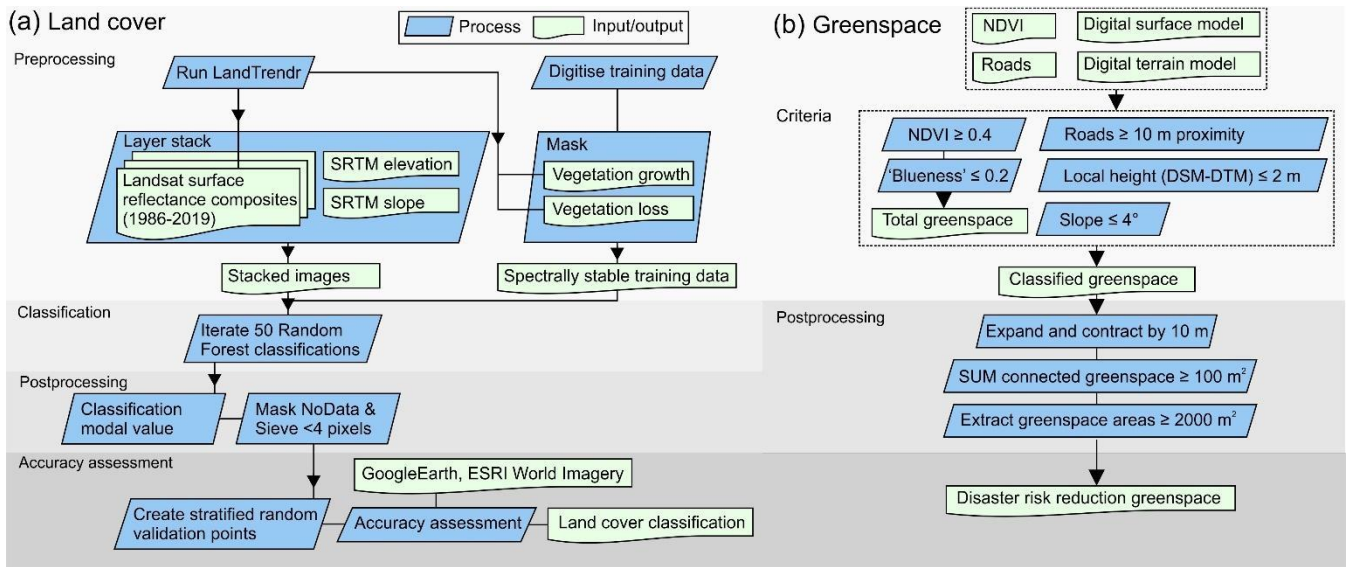
196 Urban growth for the period 1986 to 2020 was derived by applying a land cover classification workflow to 30 m resolution  
197 Landsat satellite imagery for the Land Cover AOI (Fig. 2a, 3a), including Landsat 4 Thematic Mapper (TM), Landsat 7  
198 Enhanced Thematic Mapper Plus (ETM+), and Landsat 8 Operational Land Imager (OLI). Landsat imagery was selected  
199 June to September to avoid cloud cover during the wet season (Domínguez-Castro et al., 2018). Therefore, seasonal spectral  
200 variations in land covers are not captured. Images were pre-processed using Landsat-based detection of Trends in  
201 Disturbance and Recovery (LandTrendr) and Google Earth Engine to create multi-image mosaics with minimal cloud cover  
202 using a medoid pixel composite (Gorelick et al., 2017; Kennedy et al., 2018). Training data were manually digitised as 500  
203 polygons (median polygon area of 5,400 m<sup>2</sup>) with reference to the 1986 image using four classes: 1) urban, 2) woodland, 3)

204 scrub vegetation and bare ground, and 4) agriculture and grassland. Training data were masked using the normalised  
205 difference vegetation index (NDVI) vegetation loss and growth masks that are output from LandTrendr to leave areas of  
206 training data that were spectrally consistent through time (1986–2020). Landsat composites were stacked with elevation and  
207 slope layers derived from the 30 m Shuttle Radar Topography Mission (SRTM) digital elevation model (DEM) (Farr et al.,  
208 2007) since these additional variables were shown to improve land cover classification performance (Zhu et al., 2016). We  
209 used a Random Forest classification, which is a decision tree approach popular for land cover classifications owing to their  
210 high accuracy, broad data handling, and low sensitivity to training data noise (Rodriguez-Galiano et al., 2012; Zhu et al.,  
211 2016). The Orfeo Toolbox Random Forest classifier (Inglada and Christophe, 2009) (Table S1) was run 50 times for each  
212 time period using 200 trees and a random sample of training data to account for imbalance between classes (Millard and  
213 Richardson, 2015) (Table S1). The modal value was used to produce the final classification map, which was accuracy  
214 assessed using an independent stratified random sample of 200 reference points in each class created using high resolution  
215 satellite imagery (Fig. S2). High resolution multispectral satellite imagery was not available in the 1980s, which reduces  
216 classification confidence in training and reference data, however, a panchromatic ~1 m resolution aerial orthophoto of Quito  
217 in 1977 from Instituto Geográfico Militar (1977) was used for reference. The accuracy assessment was used to produce an  
218 error-adjusted area and confidence interval of each land cover classification (e.g. Olofsson et al., 2013; Olofsson et al.,  
219 2014).

220

221 Future urbanisation scenarios in Quito were assessed with reference to Bonilla-Bedoya et al. (2020b) and Salazar et al.  
222 (2020). Both studies used predictor variables to model future urbanisation scenarios in Quito. Salazar et al. (2020) present a  
223 scenario to the year 2050, whereas Bonilla-Bedoya et al. (2020b) define an ‘urbanisation probability’ without a scenario end  
224 date. Nonetheless, the spatial trends in both studies are similar. Predictors used to derive urbanisation probability included  
225 biophysical (e.g. precipitation, slope, and altitude), land cover and management (e.g. protected areas), infrastructure and  
226 services (e.g. road network), socioeconomic (e.g. land value), and landscape metrics (e.g. landscape patch size and shape)  
227 (Bonilla-Bedoya et al., 2020). We used ‘high’ (urbanisation probability: 55–79 %) and ‘very high’ (urbanisation probability:  
228 79–100 %) classes from Bonilla-Bedoya et al. (2020b) in this study (Fig. S3) to evaluate future land cover scenarios and the  
229 intersection of urban areas with hazards.

230



231  
232 **Figure 3: (a) Land cover classification and accuracy assessment workflow. (b) Classification of greenspace that could potentially**  
233 **contribute to disaster risk reduction (DRR), herein 'DRR greenspace'.**

234 **3.2 Topography**

235 The 30 m SRTM DEM was used to extract statistics on the elevation and slope within the land cover change area of interest  
236 (AOI), which encompasses the smaller city AOI (Fig. 2a). A higher resolution (2 m and 10 m) DEM and orthoimagery was  
237 created for a smaller AOI (Fig. 2a), which bounded the Administrative Level 3 Parishes of Quito, Cumbaya, Llano Chico,  
238 Calderon (Carapungo), Conocoto, Zambiza, and Nayon. This AOI was covered by tristereo Pleiades imagery, which were  
239 acquired on five separate dates (5<sup>th</sup> November 2019, 28<sup>th</sup> January 2020, 9<sup>th</sup> February 2020, 6<sup>th</sup> June 2020, and 28<sup>th</sup> July 2020)  
240 in both panchromatic (~0.7 m) and multi-spectral (~2.8 m RGB and Near Infrared) modes (Table S2). Tristereo acquisitions  
241 produce elevation models with lower uncertainties compared to bistereo acquisitions due to greater point cloud densities  
242 afforded by the extra viewing angle (Zhou et al., 2015). All imagery was delivered with radiometric processing to reflectance  
243 and processed using rational polynomial coefficients (RPCs) without ground control points (GCPs) (e.g. Airbus Defence and  
244 Space, 2012; Zhou et al., 2015). Agisoft Metashape v.1.6.5 was used to process the imagery to create a DEM, digital terrain  
245 model (DTM), and orthorectified imagery. Briefly: (1) the panchromatic and multispectral imagery were aligned in one  
246 bundle to produce a sparse point cloud; (2) the sparse cloud was filtered to remove outliers using Metashape's gradual  
247 selection tools; (3) a dense point cloud was constructed using the panchromatic imagery, which was used to create a 2 m  
248 resolution DEM and (4) orthorectify the satellite imagery. Metashape's ground classification (maximum angle: 15°,  
249 maximum distance: 0.5 m, cell size: 50 m) was applied to the dense cloud and used to create the DTM. An additional DSM  
250 was output at 10 m resolution to reduce data gaps for deriving a Topographic Wetness Index (TWI) (Section 3.3).

252 Since the Pleiades DEM was processed without GCPs, we assessed the accuracy using Ice, Cloud and land Elevation  
253 Satellite (ICESAT-2) altimetry data. ICESAT-2 data has an expected vertical accuracy that is lower than the error expected  
254 from a Pleiades DEM created without ground control points ( $> 3\text{--}5\text{m}$ ) (Passalacqua et al., 2015; Markus et al., 2017) and  
255 was therefore used as an independent validation check. We extracted High Confidence returns from the Advanced  
256 Topographic Laser Altimeter System (ATLAS) instrument ATL03 Global Geolocated Photon Height data acquired 6<sup>th</sup>  
257 December 2018 to 3<sup>rd</sup> June 2020 that intersected with the Pleiades data (Neumann et al., 2019; Neumann et al., 2020).  
258 Photons were filtered to exclude slopes steeper than  $20^\circ$  and aggregated into 5 m grid cell mean values. Cells containing  $\geq 2$   
259 photons with an elevation range  $\leq 1$  m, were carried forward for the validation ( $n = 11,922$ ). We coregistered the Pleiades  
260 DEM and gridded ICESAT-2 data following the  $x, y, z$  shift correction of Nuth and Kääb (2011) and the difference in  
261 elevation values were compared. The mean vertical difference between the ICESAT-2 and Pleiades data was 0.38 m (one  
262 standard deviation: 1.32 m) with a normalised median absolute deviation of 0.84 m.

### 263 3.3 Hazards

264 Information on natural hazards affecting Quito were collated from published sources and Ecuador's Open Government data.  
265 We used a global landslide susceptibility model that was validated against local and global landslide inventories, with an  
266 emphasis on rainfall-triggered events (Kirschbaum et al., 2016; Stanley and Kirschbaum, 2017). Landslide susceptibility was  
267 ranked on a scale of 1 (low) to 5 (high) and the model combined data on slope, faults, geology, forest loss, and road  
268 networks, aggregated to  $\sim 1$  km grid cells (Stanley and Kirschbaum, 2017). Open Government records of 'Accidents' 2006–  
269 2017 were used to identify the geographic distribution of mass movement events ( $n = 1,321$ ), which were compared to the  
270 global landslide susceptibility model (Fig. S4) (Ministry of Territory, Habitat and Housing., 2020). We masked Class 5  
271 (high) of the landslide susceptibility model out of the future urbanisation scenario of Bonilla-Bedoya et al. (2020b) to create  
272 a restricted scenario of urban growth, which reflects DMQ's vision to remove high risk areas from future land occupation.  
273 We also excluded development on the slopes of Pichincha volcano (as unrealistically inaccessible given steep slopes) and  
274 included an area of development spanning the Metropolitan District boundary in the south (Fig. S3). We refer to the original  
275 scenario of future urbanisation and the modified scenario as F-U and M-U respectively. Information on volcanic hazards  
276 were obtained from the Geophysical Institute of the National Polytechnic School (IG-EPN) through the National Information  
277 System (SNI) (SNI, 2020). Spatial variation in earthquake hazard across Quito was not explored in this study due to the  
278 coarse resolution ( $\sim 10$  km) of available hazard information (Fig. S1). However, the high regional seismic hazard (Alvarado  
279 et al., 2014; Pagani et al., 2018) motivates our city-wide analysis of greenspace.

280

281 The 10 m Pleiades DEM was hydrologically corrected by breaching sinks (Lidberg et al., 2017), using the *Breach*  
282 *depressions least cost tool* of Whitebox 1.4.0. The breached DEM was used to derive a TWI, which was intersected with  
283 flood events in the Open Government database ( $n = 1,274$ ) to assess whether high TWI values correspond to greater

284 incidences of flood events, and therefore was indicative of potential flood hazard (Jalayer et al., 2014; Kelleher and  
285 McPhillips, 2020).

286

$$287 \quad TWI = \ln\left(\frac{a}{\tan\beta}\right) \quad (1)$$

288

289

290 where  $a$  represents the specific catchment area and  $\tan\beta$  represents the local DEM slope. Therefore, the TWI describes the  
291 tendency for a cell to accumulate and evacuate water (Beven and Kirkby, 1979; Manfreda et al., 2011; Mattivi et al., 2019).

292 We assumed a positional uncertainty radius of 20 m in the flood event records based on the observed positional spread of  
293 recorded traffic collisions at road junctions in the same database (Fig. S5). The maximum TWI value within a 20 m radius of  
294 the recorded point was extracted and compared to the TWI for a random sample of 10,000 points to test whether there was a  
295 statistically significant difference in the TWI at locations of flood events (e.g. Kelleher and McPhillips, 2020). Notably, this  
296 method does not account for the subsurface drainage network present in an urban setting, and therefore represents an  
297 assumption that this subsurface drainage network is overwhelmed during the flood event, such that all flow passes over the  
298 DEM (Kelleher and McPhillips, 2020).

### 299 **3.4 Greenspace**

300 Orthorectified multi-spectral Pleiades imagery was pansharpened in ArcGIS Pro 2.6.0 using the Gram-Schmidt algorithm  
301 and Pleiades sensor band weights to create a four-band (red, green, blue, and near infrared (NIR)) 0.5 m resolution multi-  
302 spectral image. Quito's vegetated greenspace distribution was mapped using the NDVI applied to the NIR and red bands of  
303 the pansharpened Pleiades satellite imagery (Fig. 3b):

304

$$305 \quad NDVI = \frac{(NIR - Red)}{(NIR + Red)} \quad (2)$$

306 Negative NDVI values correspond to areas lacking vegetation, whereas increasingly positive values represent healthy  
307 vegetation (Tucker et al., 1981; Pettorelli et al., 2005). In some cases, shadowed areas, for example due to buildings, display  
308 similar NDVI values to vegetation (Leblon et al., 1996; Yamazaki et al., 2009). We therefore used 100 randomly sample  
309 patches (200×200 m) to evaluate the NDVI classification with reference to the pansharpened Pleiades orthoimage. Incorrect  
310 classifications had a small overall impact, accounting for 0.4 % of the evaluated NDVI area (Table S3) with a mean patch  
311 size of 13±16 m<sup>2</sup>. Bright blue roofs also displayed a high NDVI value and were masked out using a simple 'blueness' index  
312 of values ≤ 0.2, which was derived through manual inspection of blue roofs:

313

$$314 \quad Blueness = 2 \times Blue - Red - Green \quad (3)$$

315

316 Whilst global coverage and daily observation is possible with the paired constellation, Pleiades imagery is not routinely  
317 acquired nor open access. Therefore, we also compared Pleiades NDVI values with those from an open access Sentinel-2  
318 image acquired 6<sup>th</sup> February 2020 with the aim of testing their consistency, noting that whilst the spectral bands overlap, the  
319 bandwidth of Pleiades is greater (Pleiades: red 590–710 nm, NIR 740–940 nm, Sentinel-2: red 649–680 nm, NIR 780–886  
320 nm).

### 321 **3.4.1 Disaster risk reduction (DRR) greenspace**

322 Greenspaces potentially suitable for providing safe spaces and contributing towards disaster risk reduction were identified  
323 using an EO-based workflow (Fig.3b) for areas within 800 m (accessible within a ~10-minute walk) (e.g. Dou and Zhan,  
324 2011; Jeong et al., 2021) of populations in Quito’s urban extent. The workflow identified greenspace: (1) that is vegetated,  
325 (2) greater than 10 m from a road to exclude road verges; (3) with slope  $\leq 4^\circ$  to provide a suitable gradient for ‘safe spaces’  
326 (Kilci et al., 2015; Liu et al., 2011); and (4) with a local height ( $\leq 2$  m) to identify open ground and exclude raised vegetation  
327 such as trees. Expansion and contraction buffers of 10 m were applied to connect adjacent patches of greenspace into  
328 greenspace ‘zones’, which for example could represent multiple patches of classified greenspace within a park. All areas of  
329 greenspace with a patch size  $\geq 100$  m<sup>2</sup> within these zones were summed and zones totalling  $\geq 2000$  m<sup>2</sup> of greenspace were  
330 classified as ‘potential DRR greenspace’. Space requirements in a disaster situation are dynamic; however, a 100 m<sup>2</sup> patch  
331 size is recommended to accommodate two people with communal space (cooking, access, facilities etc) in a camp-style  
332 settlement following guidelines in the Sphere Humanitarian Charter and Minimum Standards in Humanitarian Response  
333 Handbook (Anhorn and Khazai, 2015; Sphere Association, 2018). Zones of 2000 m<sup>2</sup> approximate one quarter to one third of  
334 a professional football pitch so could be expected to already exist as functional greenspaces (e.g. recreation parks) in an  
335 urban environment. These spaces were evaluated alongside a list of safe spaces designated by DMQ for use in an earthquake  
336 event (Metro Ecuador, 2019)(Table S4), in conjunction with population data projected to 2019 and socioeconomic  
337 classification data (Instituto Geográfico Militar, 2019). These socioeconomic classifications characterise a continuum of  
338 education, income, and lifestyle factors into five classes, ranging from ‘high’ to ‘low’, where ‘low’ represents basic  
339 education and limited household facilities such as rubbish collection and plumbing, whereas ‘high’ represents higher  
340 education, and houses or apartments that are provisioned with state services (Instituto Geográfico Militar, 2019).

### 341 **3.4.2 Greenspace capacity**

342 Quito’s 2019 population data (Instituto Geográfico Militar, 2019) were used to assess the population capacity of all DRR  
343 greenspace (3.4.1) in the event that they were to be used for accommodation following a disaster such as an earthquake. We  
344 assessed the capacity of two types of greenspaces: (1) DRR greenspace that overlapped with DMQ designated greenspaces,  
345 which included city parks and safe spaces (3.4.1), and (2) all DRR greenspaces identified in this study that were either  
346 designated or undesignated. These two scenarios therefore represent the DRR capacity based on current designations (1),

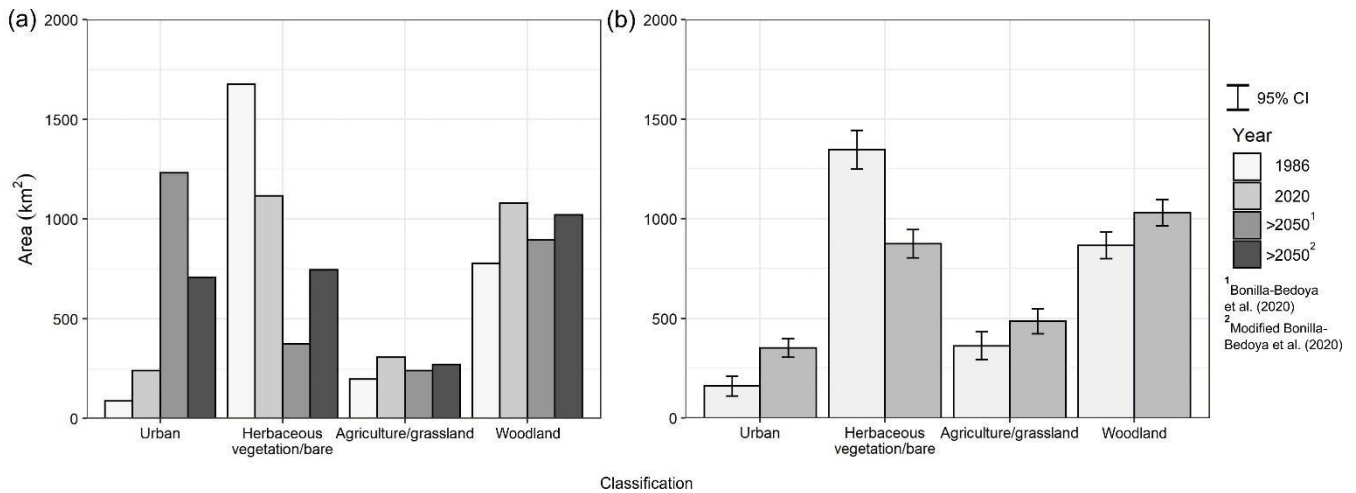
347 compared to the potential maximum capacity (2). We considered two separate cases of populations within 800 m and 1600 m  
348 network buffers of each greenspace. For each scenario, we used a network analysis to assign population demand points to  
349 each greenspace based on their proximity, up to the maximum buffer distance. The network was constructed as a grid at 100  
350 m resolution and considered population demand points also gridded at 100 m resolution, which were uniformly  
351 disaggregated from census polygons. The number of people that could be accommodated in each greenspace depends on the  
352 capacity of the space, and the population demand in the surrounding buffer. We considered capacities based on Sphere  
353 Association (2018) guidelines, which suggest an allocation of 45 m<sup>2</sup> per person (recommended amount per person  
354 accounting for communal facilities and infrastructure in an emergency shelter setting) and 3 m<sup>2</sup> per person (minimum living  
355 space per person). All demand within the buffers was allocated to the closest greenspaces, therefore excess demand was  
356 reported as overcapacity. We did not consider the possibility of people moving greater distances around the city to distribute  
357 the population demand more equally, which could occur following an initial disaster situation, or that only a fraction of the  
358 population would require access to refuge space in a disaster situation. Considering potential policy consideration, we also  
359 used a maximum capacitated coverage network analysis (e.g. Anhorn and Khazai, 2015) with the same datasets to find the  
360 ‘top ten’ DRR greenspaces in Quito based on a minimum space requirement of 3 m<sup>2</sup> per person and a travel distance of 800  
361 m.

## 362 **4 Results**

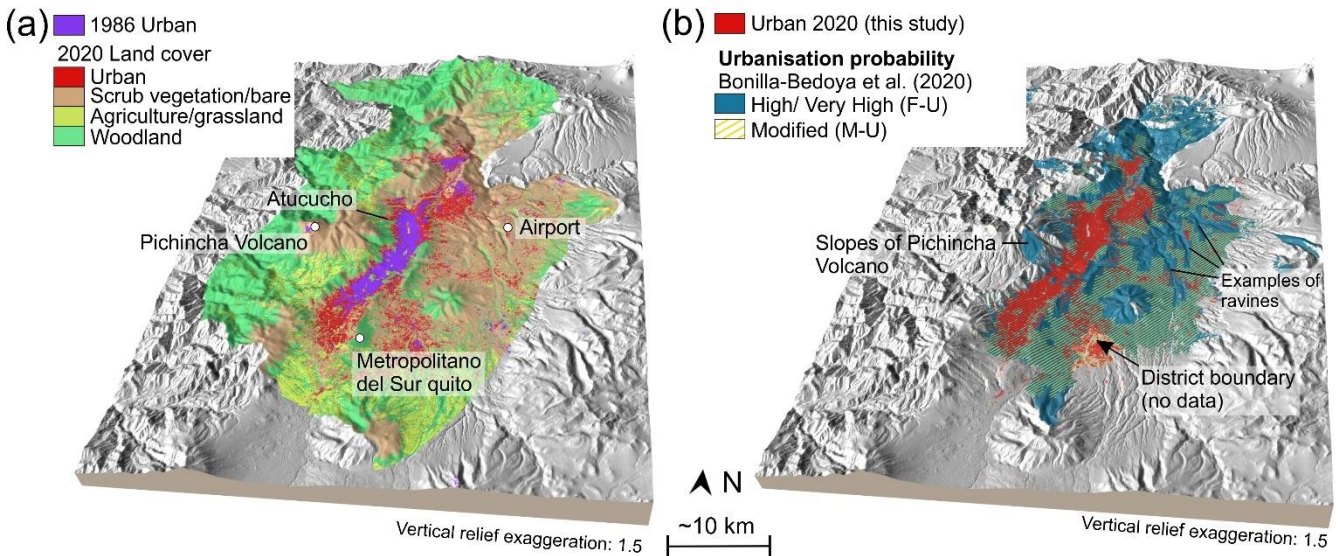
### 363 **4.1 Urban growth**

364 Our land cover classifications showed that the urban area of Quito expanded ~192 km<sup>2</sup> over the study period, more than  
365 doubling from 160±50 km<sup>2</sup> in 1986 to 352±47 km<sup>2</sup> in 2020 (Fig. 4, Table S5). Urban expansion was primarily aligned along-  
366 valley (north south) and eastward (Fig. 5a), into areas of previously scrub vegetation/bare and agricultural/grassland classes.  
367 The future urbanisation scenario of Bonilla-Bedoya et al. (2020b) covered an urban area of 1,232 km<sup>2</sup> (F-U), whereas the M-  
368 U scenario covered 705 km<sup>2</sup> (Fig. 4a), which was still double the observed 2020 urban area. Future urbanisation in the  
369 modelled scenarios was predominantly eastward, where lower density urbanisation interspersed with the scrub  
370 vegetation/bare ground class was already apparent in 2020 (Fig. 5). The area of woodland and agriculture/grassland classes  
371 also increased 1986–2020. A notable example of afforestation (4.8 km<sup>2</sup>) was the park Metropolitano del Sur, which is  
372 located on the southeast of the city limit (Fig. 5a).

373



374  
 375 **Figure 4: (a) Mapped land cover classification results for 1986 and 2020 alongside modelled future land cover from two scenarios<sup>(1, 2)</sup> using data from Bonilla-Bedoya et al. (2020). (b) Error-adjusted (e.g. Olofsson et al., 2013; Olofsson et al., 2014) land cover**  
 376 **classification results from 1986 and 2020.**  
 377

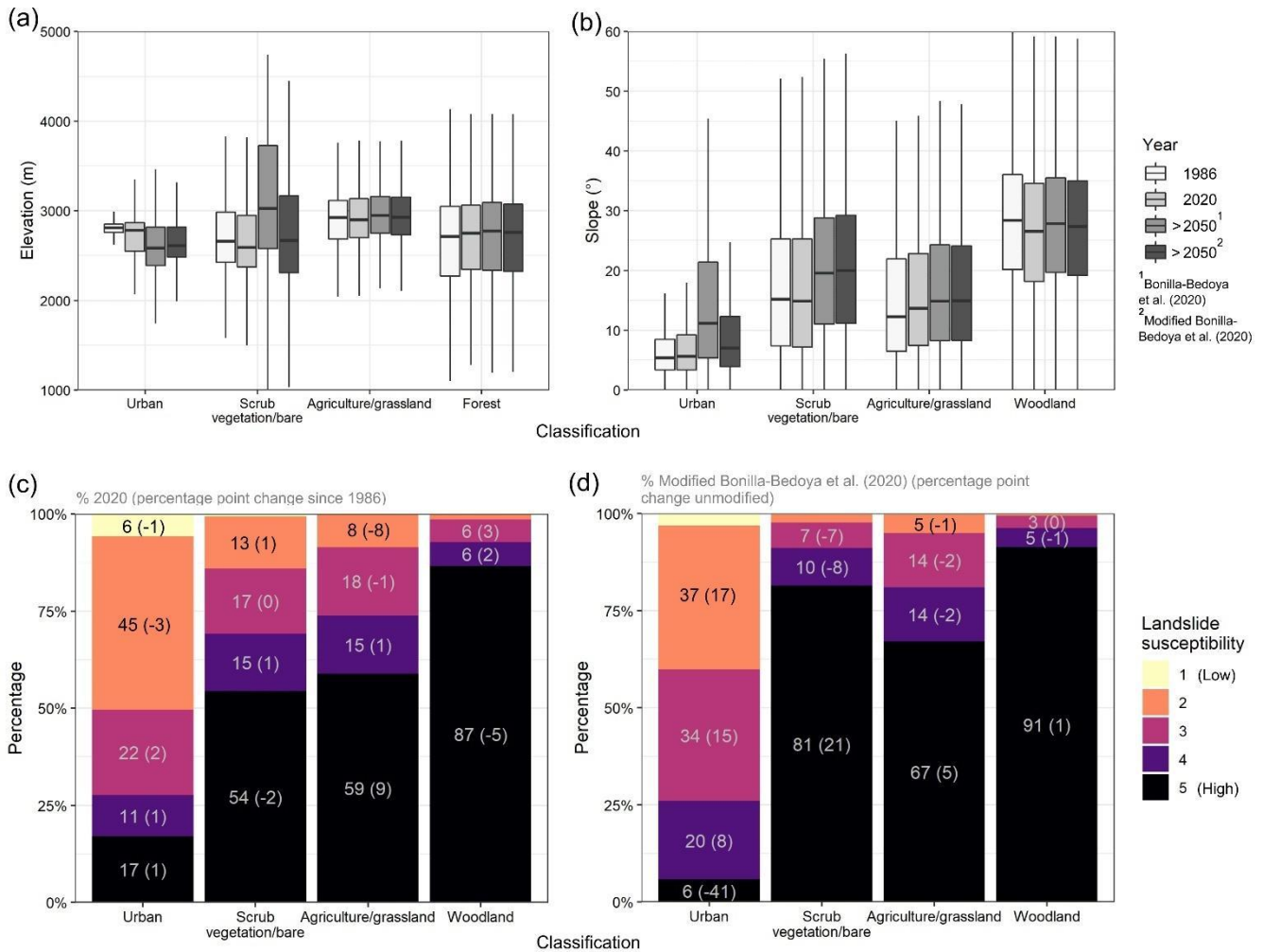


380  
 381 **Figure 5: (a) 3D perspective showing urban growth 1986–2020 and land cover. (b) Quito's urban area in 2020 compared to modelled future urbanisation (F-U) (Bonilla-Bedoya et al., 2020) and a modified scenario (M-U). Background is a hillshaded**  
 382 **SRTM DEM.**  
 383

384 The median elevation of Quito's urban extent in 2020 (2,780 m) was similar to 1986 (2,810 m); however, the city covered a  
 385 broader elevation range in 2020, tending towards lower elevations (Fig. 6a), which was also apparent for the F-U and M-U  
 386 scenarios. The urban class displayed the smallest spread of values for topographic slope (Fig. 6b). Here, the median slope of



387 the urban class was  $\sim 5^\circ$  in 1986 and 2020, however this increased to  $11^\circ$  and  $7^\circ$  in the F-U and M-U scenarios respectively,  
 388 in addition to a broader spread of slope values. Woodland featured the highest median slope of all land cover classes ( $\sim 28^\circ$ )  
 389 and a comparable median elevation to the urban class ( $\sim 2700$ – $2800$  m).  
 390



391  
 392 **Figure 6: Elevation (a) and slope (b) characteristics of the classified and modelled land cover scenarios. Boxes show the**  
 393 **interquartile range and the median (horizontal line). Lines show values within 1.5 times the interquartile range. Outliers are not**  
 394 **shown. (c) 2020 land cover intersections with landslide susceptibility and the percentage points change since 1986. (d) Future land**  
 395 **cover intersections with landslide susceptibility using modified urbanisation probability (M-U) of Bonilla-Bedoya et al. (2020, and**  
 396 **the difference compared to the unmodified scenario (F-U).**

#### 397 4.2 Intersection with hazards

398 Landslides are one of the most common natural hazards in Quito (DMQ, 2018). We found good spatial association between  
 399 observations of landslide events in Ecuador’s Open Government database (2006–2017) and a landslide susceptibility model

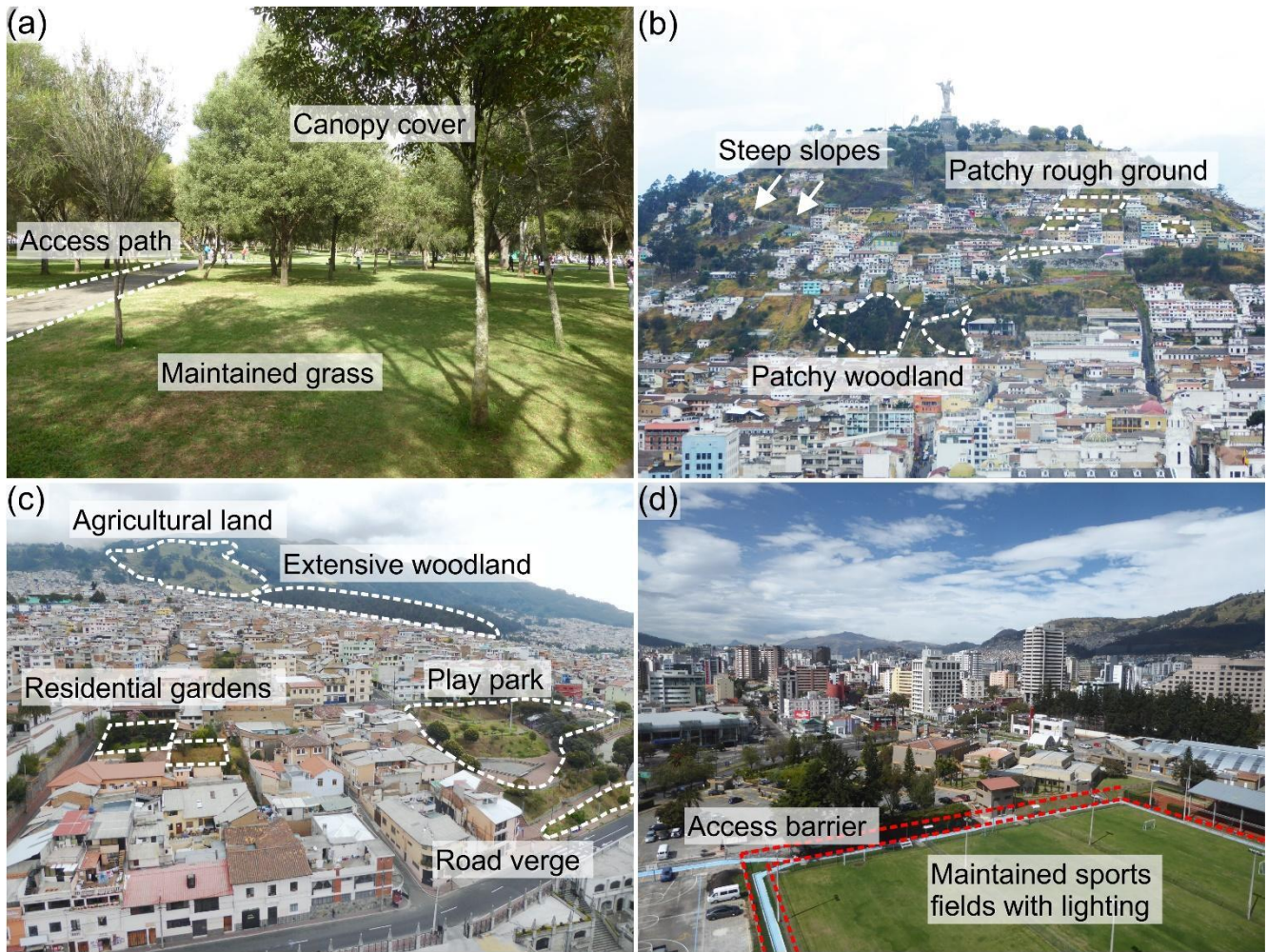
400 (Stanley and Kirschbaum, 2017) (Fig. S4). Of 1,321 recorded events, 82% (n = 1,089) fell within landslide susceptibility  
401 categories 3–5, of which 44% (n = 576) were in the highest category (5). Ten events were observed in the lowest category  
402 (1). We observed a small change in the landslide susceptibility of the urban class 1986–2020. Here, the urban area in the  
403 highest landslide susceptibility categories (4 and 5) increased by 2 percentage points 1986–2020 (Fig. 6c). The largest  
404 change was observed in the agriculture/grassland class, which featured a 9-percentage point increase in category 5 (high)  
405 landslide susceptibility. Woodland mostly occurred within the highest landslide susceptibility category 5 (87%) (Fig 6c).  
406 Regarding future urbanisation, the M-U scenario restricted future urbanisation in landslide susceptibility category 5,  
407 therefore the observed percentage of urban area in category 5 (6%) was notably lower than in the F-U scenario (47%), which  
408 did not enforce any restrictions.

409

410 Flood events in Quito that were recorded in Ecuador’s Open Government database were evaluated alongside a TWI derived  
411 from the 10 m resolution Pleiades DEM, noting that this does not account for subsurface drainage. Median TWI values for  
412 all flood events (n = 1,274), clustered flood events where two or more events were located within 40 m of each other (n =  
413 125), and a random sample (n = 10,000), were 13.3, 14.4, and 12.1 respectively (Fig. S6). Clustered flood events, which  
414 displayed the highest TWI, could correspond to areas of nuisance flooding since multiple events are located in close  
415 proximity (Kelleher and McPhillips, 2020). Two sample independent Welch t-tests (one-tailed) showed that the difference in  
416 TWI values between all flood events and clustered floods events were statistically significantly different from the random  
417 sample ( $p < 0.05$ ). Therefore, the mean TWI value was observed to be larger in areas of flood locations compared to the  
418 random sample.

### 419 **4.3 Greenspace**

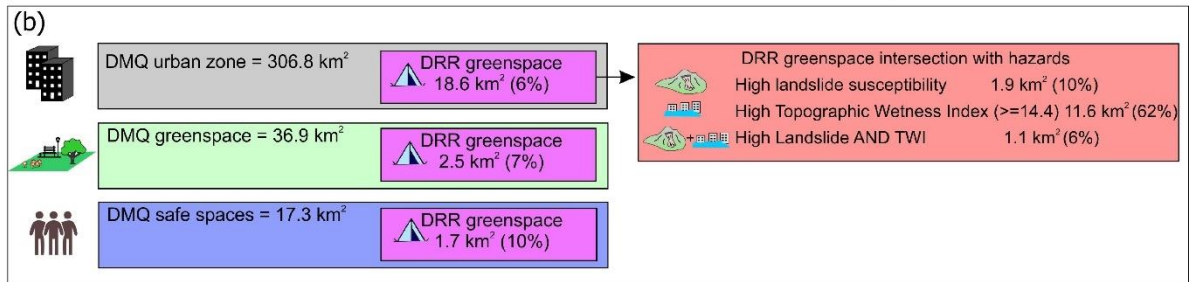
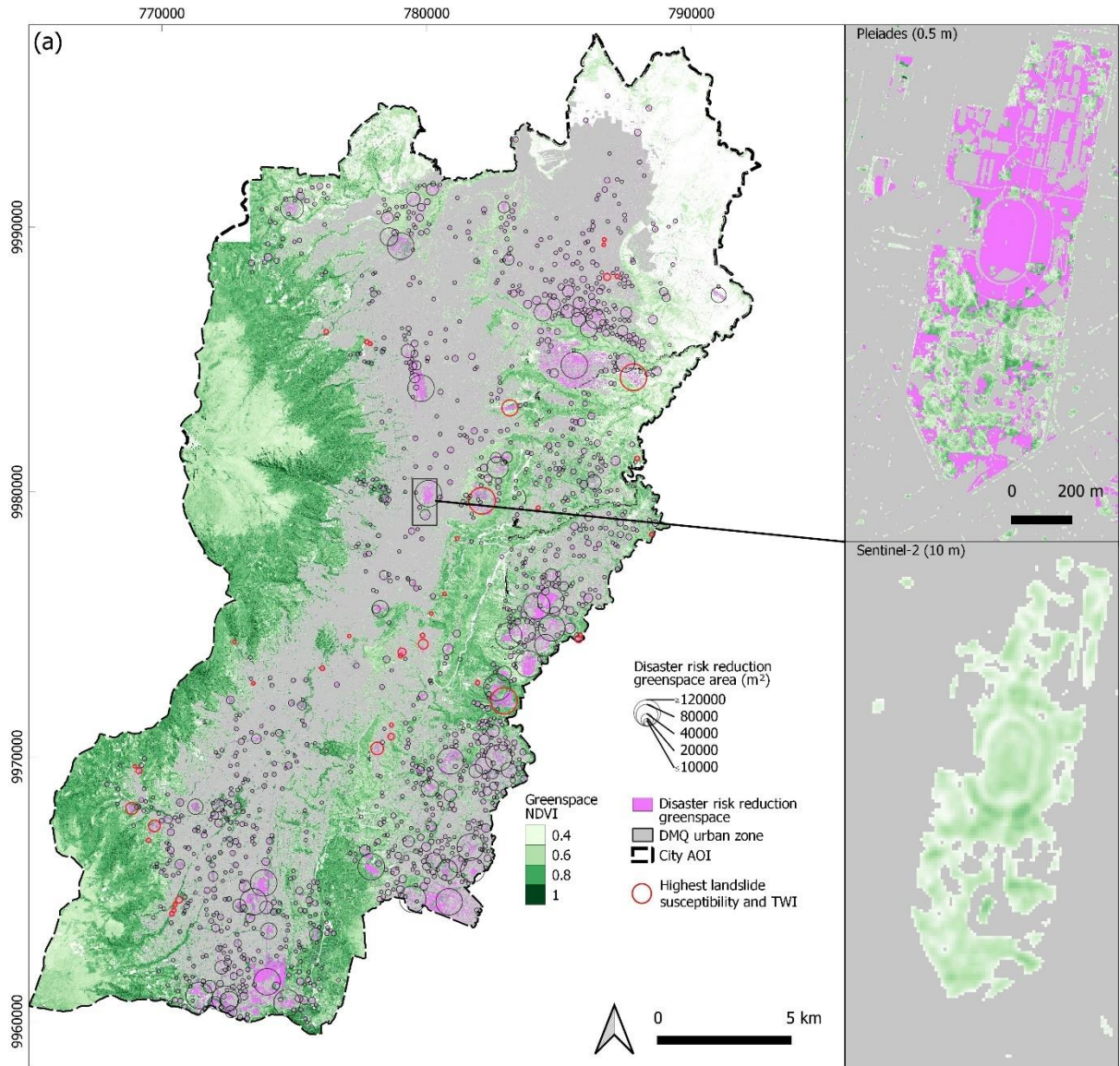
420 Quito includes multiple types of greenspace that provide ecological, social, and disaster risk reduction benefits (Fig. 1a, 7).  
421 Within our AOI, 18.6 km<sup>2</sup> of potential DRR greenspace was identified, which covered 6% of the urban zone (Fig. 8). DMQ  
422 designated greenspace had an area of 36.9 km<sup>2</sup>, of which 2.5 km<sup>2</sup> (7%) intersected with potential DRR greenspace. Similarly,  
423 DMQ designated safe spaces covered 17.3 km<sup>2</sup>, of which 1.7 km<sup>2</sup> (10%) intersected with potential DRR greenspace.  
424 Comparing DRR greenspaces with hazard information revealed that 62% of DRR greenspace intersected with areas of high  
425 TWI values ( $\geq 14.4$  (median value for clustered flood events - Section 4.2)), 10% intersected with areas of high (category 5)  
426 landslide susceptibility, and 6% intersected with both hazards (Fig. 8b).



427

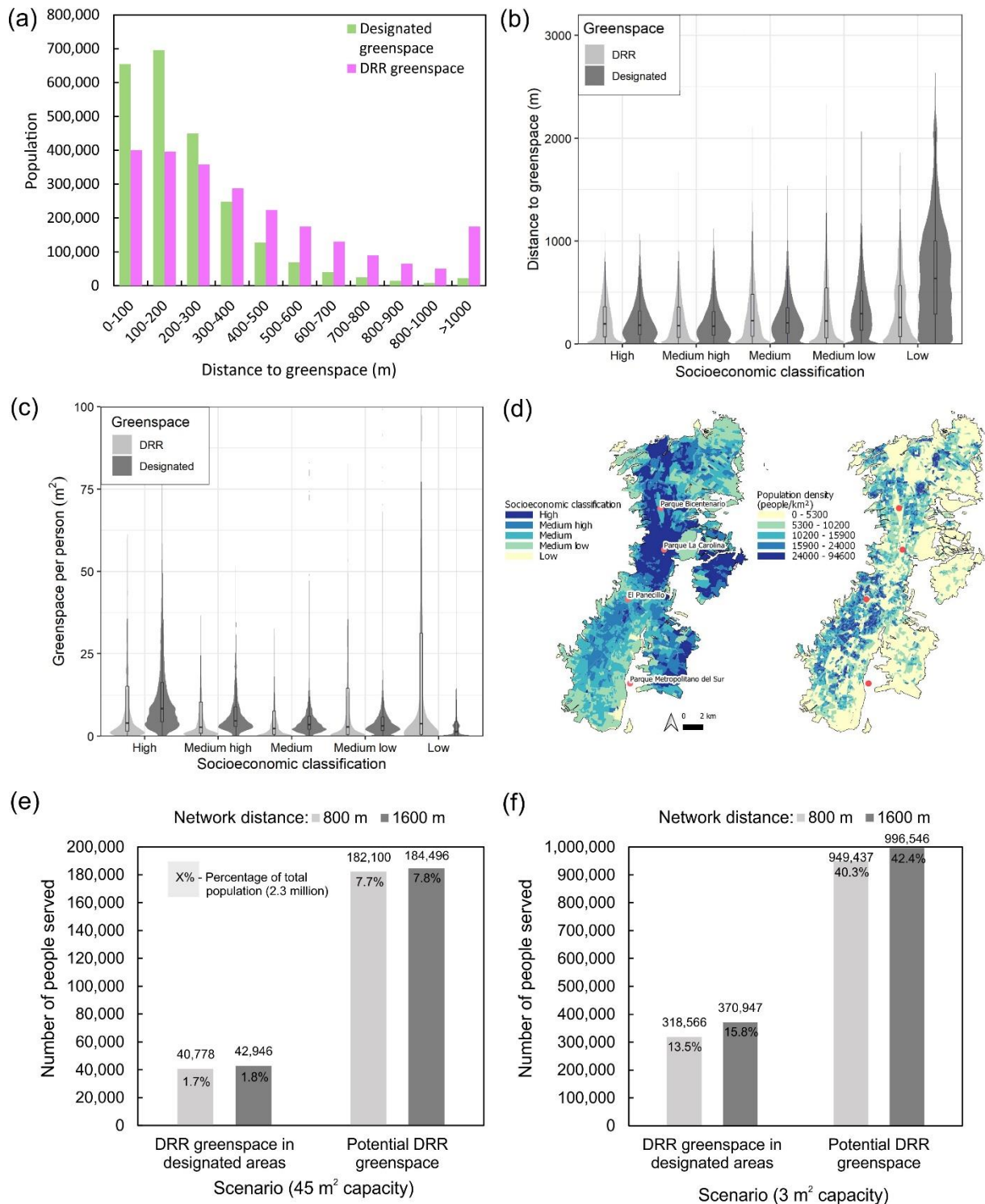
428

Figure 7: Examples of greenspace in Quito from photographs taken in October 2019 (a–d).



430 **Figure 8: Greenspace mapped using the NDVI applied to Pleiades satellite imagery shown with classified potential DRR**  
431 **greenspace (black and red circles, pink shading). Red circles indicate DRR greenspace that intersects with landslide susceptibility**  
432 **class 5 (high) and a Topographic Wetness Index value of  $\geq 14.4$  (median value for clustered flood events - Section 4.2). The inset of**  
433 **Carolina Park shows the similarity of Pleiades-derived greenspace compared to greenspace mapped using Sentinel-2 imagery. The**  
434 **Pleiades inset shows the distribution of potential DRR greenspace (pink) in Carolina Park. (b) Summary of greenspace availability**  
435 **and hazard intersections.**

436 The association between population, socioeconomic classification (Instituto Geográfico Militar, 2019), and greenspace  
437 accessibility was investigated for greenspaces  $\geq 2000$  m<sup>2</sup>. The number of people living within close proximity to designated  
438 greenspace was higher than for DRR greenspace (Fig. 9a). For example, 2.3 million (98%) of Quito's population were within  
439 800 m of a designated greenspace, compared to 2.1 million for the DRR greenspace (88%). Distance to the nearest  
440 greenspace was greater for 'low' and 'medium low' socioeconomic classifications compared to 'high' and 'medium high'  
441 (Fig. 9b). Here, the difference in median values was greatest for designated greenspace (466 m), compared to our  
442 classification of DRR greenspace (80 m). The amount of designated greenspace per person was smaller for lower  
443 socioeconomic classifications, with a median of 3 m<sup>2</sup> per person for the 'low' classification compared to 8 m<sup>2</sup> for 'high'.  
444 However, the amount of DRR greenspace was greatest for lower socioeconomic classifications, with a median of 24 m<sup>2</sup> per  
445 person for 'low' compared to 4 m<sup>2</sup> for 'high' (Fig. 9c). This reflects lower population densities on the city margins (Fig. 9d)  
446 and the persistence of agricultural land and undeveloped ground in these areas following urbanisation.



447

448

449

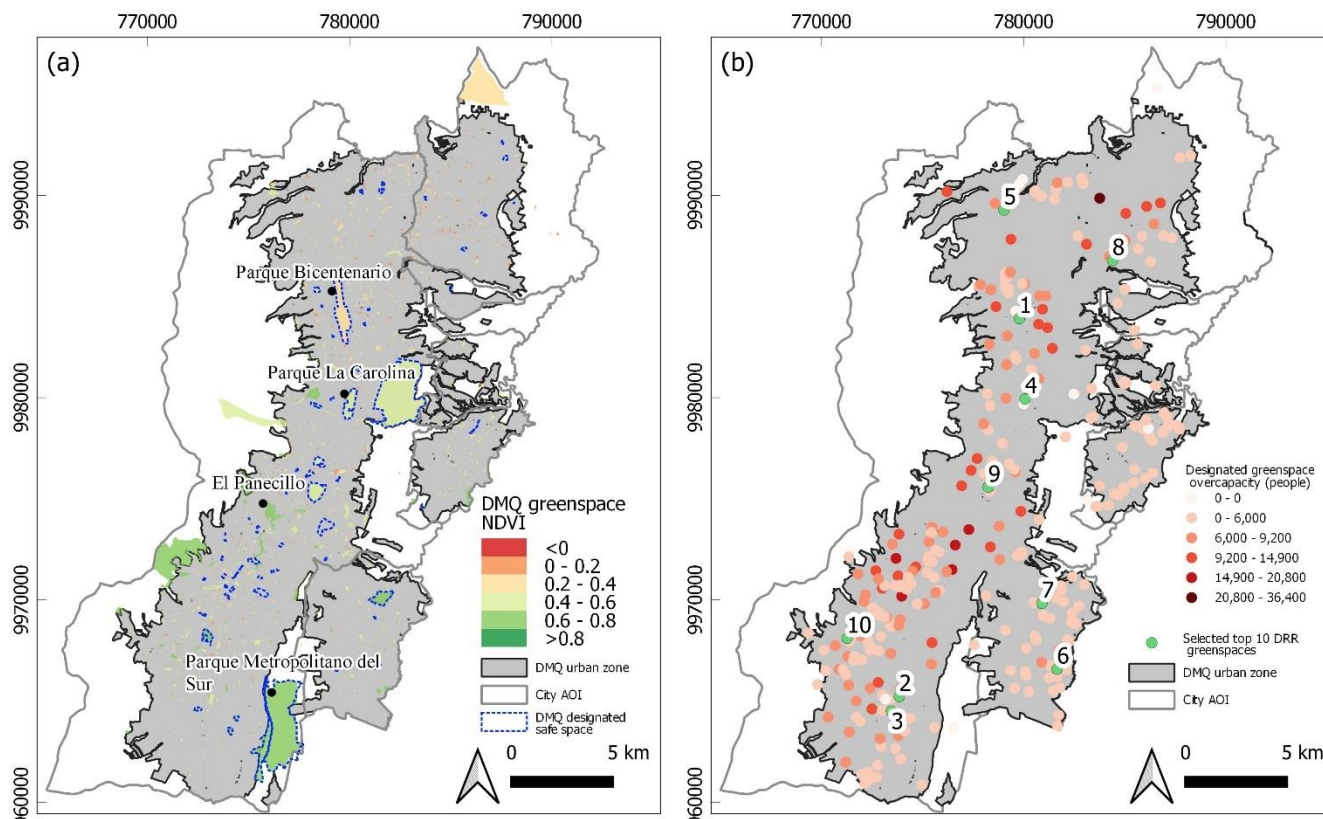
**Figure 9:** (a) Population proximity to designated and DRR greenspace. (b) Violin plot showing distance to the nearest greenspace for each socioeconomic classification. Overlaid boxplots show the interquartile range and the median (horizontal line). Lines show

450 values within 1.5 times the interquartile range. Outliers are excluded. (c) Violin plot showing greenspace per person within 800 m  
 451 for each socioeconomic classification. Boxplots are overlaid with outliers excluded and values > 100 m<sup>2</sup> per person are not shown.  
 452 (d) Spatial variation in socioeconomic classification and population density for Quito using data from Instituto Geográfico Militar  
 453 (2019). (e) Number of people that could be accommodated in DRR greenspace based on an allocation of 45 m<sup>2</sup> per person capacity  
 454 and (f) 3 m<sup>2</sup> per person capacity. (e-f) Show capacitated populations for a network distance of 800 m (light grey bars) and 1600 m  
 455 (dark grey bars) from the greenspace centroid and for DRR greenspace in designated spaces compared to all potential DRR  
 456 greenspace mapped in this study.

### 457 4.3.1 Greenspace capacity

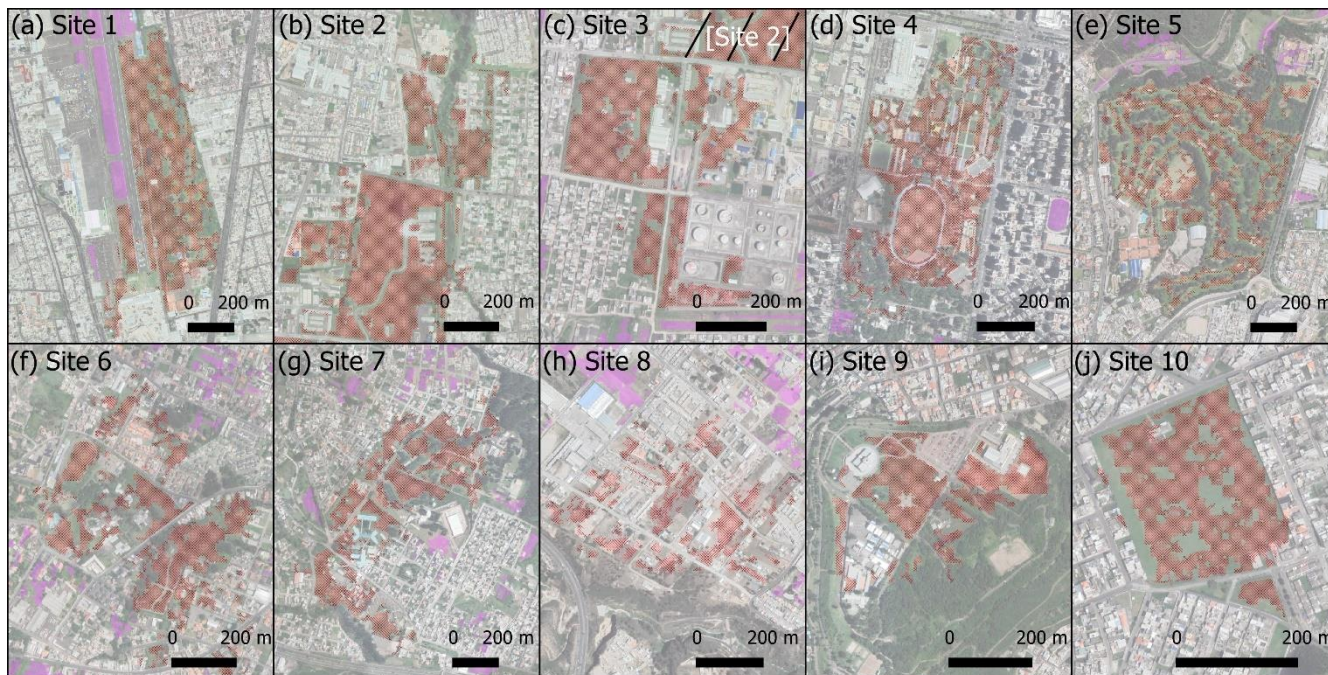
458 We assessed the capacity of each space considering the surrounding population demand. For populations within 800 m, DRR  
 459 greenspace in currently designated areas could accommodate 1.7% (40,778) of Quito's population (total 2.3 million) with an  
 460 allocation of 45 m<sup>2</sup> per person, or 13.5% (318,556) with 3 m<sup>2</sup> per person (Fig. 9 e-f, 10a). Considering all potential DRR  
 461 greenspace (Fig. 8a), these values are 7.7% and 40.3% respectively (Fig. 9e-f). The top ten DRR providing greenspaces are  
 462 shown in Fig. 10b and Fig. 11. Eight of these spaces overlap fully or partially with currently designated greenspaces or safe  
 463 spaces and two did not (Fig. 11). Of these 278 currently designated spaces, only 10 were not over capacity based on the  
 464 population demand (Fig. 10b).  
 465

465



466

467 **Figure 10: (a) Designated green areas and safe spaces (blue dashed polygons) from Open Government data and their mean NDVI**  
 468 **extracted using Pleiades satellite data. (b) Overcapacity of DRR greenspace in currently designated greenspaces or safe spaces.**  
 469 **Green markers show the top 10 DRR greenspaces based on a maximum capacitated coverage model.**  
 470



Site locations (designated greenspace/safespace (Y-Yes/N-No/ P-Partially))  
 Site 1 (Parque Bicentenario - Quito): -78.4864,-0.1454 (Y)  
 Site 2 (Unknown grassland - Quito): -78.5397,-0.3143 (P)  
 Site 3 (Unknown grazing grassland - Quito): -78.5432,-0.3208 (N)  
 Site 4 (Parque La Carolina - Quito): -78.4839,-0.1813 (Y)  
 Site 5 (Quito Tennis y Golf Club - Quito): -78.4932,-0.0968 (N)  
 Site 6 (Parque Recreacional La Moya - Conocoto): -78.4697,-0.3020 (P)  
 Site 7 (Parque Metropolitano La Armenia - Conocoto): -78.4764,-0.2726 (P)  
 Site 8 (El Carmen - Calderon (Carapungo)): -78.4451,-0.1194 (P)  
 Site 9 (Parque Itchimbia - Quito): -78.5002,-0.2207 (Y)  
 Site 10 (Unknown grazing grassland - Quito): -78.5629,-0.2883 (P)  
 Background imagery © Goolele Earth 2022

471 **Figure 11. Top ten ranked DRR greenspaces (red) and other nearby DRR greenspaces (pink) derived using a maximum**  
 472 **capacitated coverage network analysis, which finds the greenspaces capable of accommodating the most people within 800 m using**  
 473 **a minimum space requirement of 3 m<sup>2</sup> per person (Section 3.4.2).**  
 474

## 475 5 Discussion

### 476 5.1 Urban growth and hazard intersections

477 Quito's historical urban expansion is largely aligned north-south, whereas future urban expansion is focussed to the north  
 478 and east (Fig.5). Our study captures a period of land occupations starting in the 1980s including the settlement of Atucucho  
 479 (Fig. 2b, 5a), which formed informally in 1988 (Testori, 2016). This occupation is visible in our land cover classification  
 480 (Fig. 5a). The formation date is labelled as 2003 in Open Government data (Fig. 2b), which likely reflects its origins as an  
 481 informal settlement that was potentially not included in official maps until 2003. In this case, satellite imagery can capture



482 the urban sprawl of a city, including occupations that may not be apparent in historical maps. However, image classification  
483 methods usually only capture 2D sprawl, and not vertical high-rise developments or redevelopments that are important for  
484 measuring exposure to natural hazards (e.g. Amey et al., 2021). Quito's past and projected urban growth has been studied by  
485 several authors in recent years (e.g. Bonilla-Bedoya et al., 2020b; Salazar et al., 2020; Valencia et al., 2020). Cross-  
486 comparisons are complicated by the use of different study areas since Quito's urban area now exceeds the designated  
487 metropolitan district boundary, which has prompted investigations to create a new district area (Salazar et al., 2021). By  
488 comparing our urban classification (year 2020) to that of Bonilla-Bedoya et al. (2020) (year 2016) within the same area of  
489 interest, we find urban areas of 213 km<sup>2</sup> and 210 km<sup>2</sup> respectively, which indicates classification consistency using EO data  
490 despite different methodological approaches.

491  
492 We observed that expansion of Quito and future projections tend towards lower elevations (Fig. 6a) and steeper slopes (Fig  
493 6b), the latter of which is associated with encroachment into areas of high landslide susceptibility (Fig. 6c, d). Limited urban  
494 expansion to the east of Quito on the steep slopes of Pichincha volcano suggests that a programme of protection to avoid  
495 encroachment is working (Vidal et al. 2015). However, several of these areas or their vicinities are inhabited because of  
496 previous land invasion dynamics that affected the peripheral green belt. They can be characterised from a spatial and  
497 socioeconomic approach as a homogeneous space, in which the less economically favoured classes experience greater  
498 possibilities of isolation from other social groups (Bonilla-Bedoya et al., 2020a). Further limiting eastward urban growth  
499 reduces the ashfall and lahar hazard in the event of an eruption (Fig. 2c) and the hazard posed by landslides (Fig. 2d).  
500 Additionally, the predominantly woodland slopes east of Quito (Fig. 5a) featured the highest landslide susceptibility scores  
501 (87% of woodland is in class 5 (High) (Fig. 6c)) and are therefore a valuable target for protection against urbanisation. Our  
502 observed decreasing elevation trend of Quito's urban area (Fig. 6a) reflects north-south and eastward expansion into lower  
503 lying flatter areas, such that at a city-scale, Quito's landslide susceptibility did not notably increase 1986–2020 (Fig. 6c).  
504 These areas are also the location of projected future expansion (Bonilla-Bedoya et al., 2020b; Salazar et al., 2020; Valencia  
505 et al., 2020), predominantly through conversion of scrub vegetation and bare ground (Fig. 5a). Notable ravines exist in these  
506 areas, therefore risk-informed planning to reduce encroachment on steep slopes, which was reflected in our M-U future  
507 urban scenario, is desirable to minimise landslide risk to future developments. These areas are also likely to be most  
508 susceptible to multi-hazards such as rainfall triggered lahar remobilisation or landslides, and flood and earthquake triggered  
509 landslides (Gill and Malamud, 2017). Similarly, the filling of ravines from the seventeenth century onwards restricts the  
510 drainage capacity during intensive rainfall and increases flood risk (Aragundi et al., 2016), therefore, incorporating  
511 additional DRR greenspaces here to attenuate runoff and store water could be beneficial.

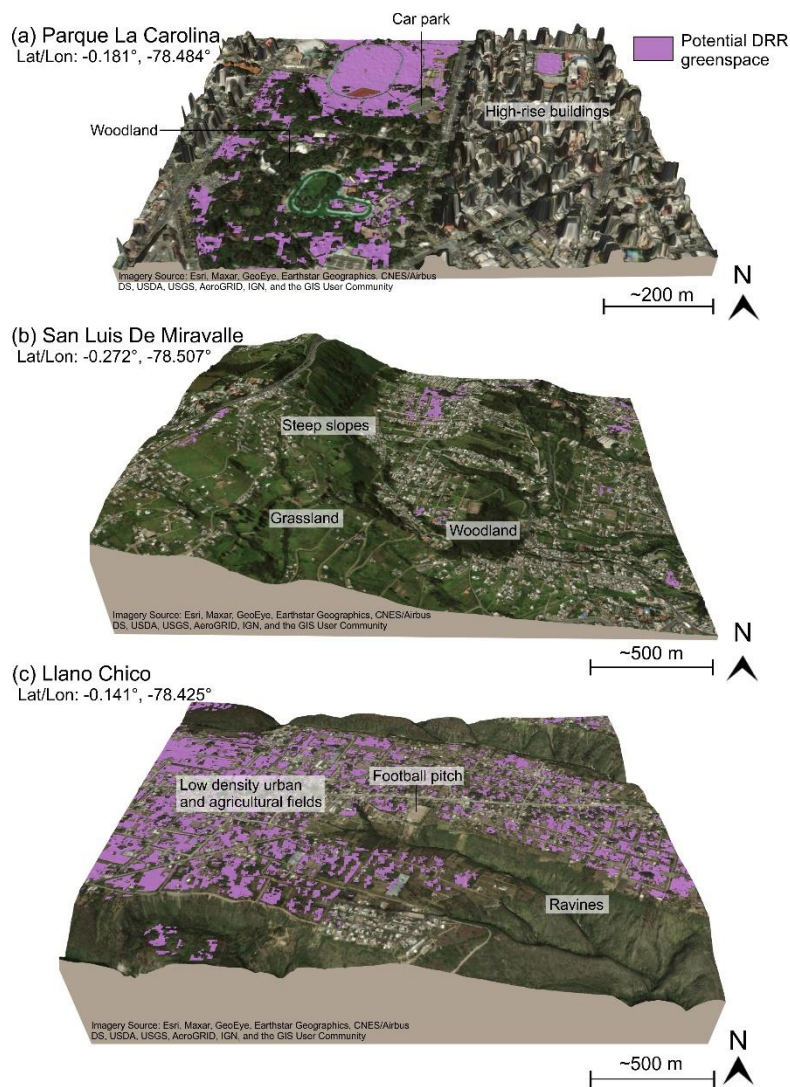
512  
513 While risk-informed urbanisation can mitigate some hazards such as landslides, an intensive earthquake hazard exists in  
514 Quito (Fig. S1), such that urban risk reduction requires building resilience at community to city-wide levels (Alvarado et al.,  
515 2014; Valcárcel et al., 2017). A key element of resilience is the access to 'safe spaces' following an earthquake event where

516 communities can avoid damaged buildings and infrastructure and receive emergency aid (Sphere Association, 2018). These  
517 spaces are increasingly viewed within a broader network of benefits to society and ecosystems (e.g. Fig.1a), and framed  
518 within Eco-DRR strategies (UNDRR, 2020). We therefore evaluated greenspaces in Quito that could offer DRR capabilities  
519 by both considering existing designated greenspaces and assessing other non-designated greenspaces.

## 520 **5.2 Greenspace**

521 Our study was designed to identify the basic requirements for sites that could be designated or developed as DRR greenspace  
522 using an earth-observation based methodology that could be adapted and applied to other cities. This is timely since  
523 greenspace is becoming increasingly desirable to improve environment quality, contribute to addressing climate breakdown,  
524 and greenspace within Eco-DRR strategies can simultaneously mitigate against multiple hazards (Onuma and Tsuge, 2018;  
525 McVittie et al., 2018; Sudmeier-Rieux et al., 2021). Our DRR greenspace primarily addresses the basic requirements of  
526 people-space and amenable topography for medium- to long-term accommodation requirements, such as following a major  
527 earthquake. Examples are shown in Fig. 12 for areas in central Quito and on the periphery. Regarding urban risk, green space  
528 in Quito has been thought of from the perspective of threat. For example, interventions have been developed on the slopes of  
529 Pichincha from a logic of risk mitigation (Vidal et al., 2015). Recently, after the 2016 Ecuador earthquake, green and open  
530 spaces were incorporated throughout the city as safe points in case of evacuation (Rebotier, 2016) (Fig. 10a).

531



532

533 **Figure 12: 3D perspective showing examples of potential DRR greenspace identified in Quito. (a) Parque La Carolina is in central**  
 534 **Quito amongst commercial high-rise buildings. (b) San Luis De Miravalle is located on the southeast of Quito and is characterised**  
 535 **by lower density urban development and steep slopes. (c) Llano Chico is in the east of Quito with low density urban development**  
 536 **mixed with agricultural land that is bounded by steep ravines.**

537 We found that 7% (2.5 km<sup>2</sup>) of the DMQ designated greenspace was identified as potential DRR greenspace. Similarly, 10%  
 538 (1.7 km<sup>2</sup>) of the DMQ designated safe spaces intersected with our classified DRR greenspace (Fig. 8, 10a). The total area of  
 539 potential DRR greenspace within Quito was 18.6 km<sup>2</sup>, therefore large potential exists to incorporate new greenspaces into a  
 540 DRR framework, especially in the south and east of the city, which are locations of projected future expansion and where  
 541 urban expansion and population densities are lower (Fig. 5b, 9d). New designation of greenspaces could address some of the  
 542 imbalance between greenspace access since 98% (~2.3 million) of Quito's population were within 800 m of a designated  
 543 greenspace, compared to 2.1 million for the DRR greenspace (88%) (Fig. 9a). Lower socioeconomic classifications had a

544 greater distance to travel to the nearest designated greenspace, and a lower greenspace area per person overall (Fig. 9b, c),  
545 which was also observed by Cuvi et al. (2021), noting that informal developments have less access to larger designated  
546 parks. We found a median designated greenspace of 3 m<sup>2</sup> per person for the 'low' socioeconomic classification. However,  
547 the availability of potential DRR greenspace to these same communities (median of 24 m<sup>2</sup>) shows that additional  
548 designations could help address the imbalance. This is also aligned with Quito's Vision 2040 document to increase  
549 greenspace in urban areas to ~9 m<sup>2</sup> per person (DMQ, 2018). Critical to addressing these inequalities is to ensure that all  
550 formal and informal settlements are reflected in socioeconomic statistics and included in official maps.

551  
552 Although we found high accessibility of greenspace within 800 m of populations, the capacity to serve surrounding  
553 populations for emergency refuge was 1.7% considering the recommended space allocation of 45 m<sup>2</sup> per person (Fig.  
554 9a)(Sphere Association, 2018). Incorporating all additional spaces that are DRR suitable could increase this to 8%, or 40%  
555 using a minimum living allocation of 3 m<sup>2</sup> per person (Sphere Association, 2018). A network analysis producing a ranked  
556 top ten DRR greenspaces (Fig. 11) showed that eight intersected with currently designated greenspaces or safe spaces and  
557 two did not. These two spaces could be investigated for negotiating formal access to these spaces for use in an emergency,  
558 such as the golf course forming Site 5 (Fig. 11e).

559  
560 We focus on greenspace as an emergency refuge; however, these spaces can also contribute to mitigating hazards both  
561 through physical processes such as water retention or slope stabilisation (Phillips and Marden, 2005; Maragno et al., 2018;  
562 Sandholz et al., 2018), and also by their existence in places that would be hazardous if urbanised. We found that of the  
563 potential DRR greenspace identified in Quito, 62% intersected with TWI values indicative of potential flooding (section  
564 4.2), 10% with areas of high landslide susceptibility, and 6% with both hazards (Fig. 8 – red circles). Therefore, there is  
565 potential to mitigate future risk by maintaining greenspace and therefore avoiding development in potentially hazardous  
566 areas, and incorporating additional DRR greenspaces that are not exposed to hazards for use as refuges.

### 567 **5.3 Future work**

568 Our study has provided a city-wide assessment of Quito's historical and future growth projections, and the potential role of  
569 greenspace in reducing disaster risk. The first-pass analysis of greenspace suitable for DRR could be used for local  
570 community-scale evaluation and stakeholder engagement to deliver improved resilience for the city. Subsequently, the  
571 methodology could be expanded to define a continuum of greenspace suitability for DRR by incorporating other important  
572 factors including site specific suitability trade-offs such as land value, ownership, and access to water, electricity, and  
573 hospitals (Anhorn and Khazai, 2015; Hosseini et al., 2016). Similarly, we focussed on greenspaces since these spaces are  
574 most likely to be accessible and they provide multiple benefits; however, concreted grey spaces such as commercial car  
575 parks could also serve a role in providing safe spaces for DRR, particularly if a disaster event occurred during work hours.  
576 Methodological developments could include multi-temporal and potentially higher resolution datasets, for example landslide

577 susceptibility information that reflects changing land cover and therefore an evolving hazard (Emberson et al., 2020). For  
578 example, a dynamic landslide susceptibility map could consider a potentially increased landslide hazard due to road cuttings  
579 in areas undergoing urban development (Froude and Petley, 2018), and the dynamic nature of landslide hazard in response to  
580 precipitation events (Kirschbaum and Stanley, 2018). Additionally, our investigation of flood events alongside a TWI would  
581 benefit from a better understanding of the capacity and distribution of the subsurface drainage network within Quito,  
582 particularly where natural drainage channels are blocked (e.g. Aragundi et al., 2016). Nonetheless, our assumptions that all  
583 flood water would flow on the surface represents a worst-case scenario during a flood event where the artificial drainage  
584 network is at capacity.

585

586 Use of EO-based datasets broadens the applicability of our methods to other cities. Whilst other sources of multi-spectral  
587 satellite imagery (e.g. 3 m resolution PlanetScope or 10 m resolution Sentinel-2) could still delineate the types of greenspaces  
588 relevant to DRR (e.g. Fig. 8 inset), we relied on a high resolution Pleiades DEM to provide topographic relief information on  
589 the greenspace DRR suitability. Global 30 m resolution DEMs could likely substitute this in some cases, though they are  
590 potentially less suitable in densely built urban environment where flat open greenspaces are interspaced with tall buildings  
591 and trees for example (Fig. 12a), which cannot be distinguished in 30 m elevation models. Here, elevation and slope values  
592 derived from 30 m resolution DEM represent an average of features (for example buildings, cars, and trees) within the 30 m  
593 cell. Therefore, the topography of greenspaces is resolved in less detail.

## 594 **6 Conclusion**

595 In this study, we used a combination of satellite data analysis and secondary datasets to quantify Quito's historical growth,  
596 future intersection with hazards, and distribution of greenspace within the city. Quito's historical growth (~192 km<sup>2</sup> 1986 to  
597 2020) was primarily on flatter, former agricultural land, hence there was limited encroachment towards hazards of Pichincha  
598 volcano and areas of higher landslide susceptibility. However, our work shows that future urbanisation projections suggest  
599 an increasing intersection between urban areas and areas of high landslide susceptibility, which requires risk-informed  
600 planning to mitigate. General accessibility of greenspaces is high, with 98% (2.3 million) of Quito's population within 800 m  
601 of a designated greenspace and 88% (2.1 million) for the DRR greenspace classification. However, within 800 m, the  
602 capacity of currently designated greenspaces and safe spaces would only fulfil 2% of Quito's population if required for  
603 emergency refuge. Over 40% could be accommodated by incorporating new DRR greenspaces identified in this study. We  
604 also found a disparity between access to greenspaces across socio-economic classifications, with low-medium groups having  
605 less access to designated greenspace (3 m<sup>2</sup> per person for the 'low' classification compared to 8 m<sup>2</sup> for 'high'). In some  
606 cases, these low-medium groups have the greatest opportunity for future designation of DRR greenspace due to their location  
607 on the city periphery in areas of lower population density. Our workflow uses satellite data to provide a first-pass evaluation  
608 of DRR greenspace potential and could therefore be adapted for application in other urbanising cities. The results provide the

609 foundation to evaluate these spaces with stakeholders at community to city-wide scales, since promoting equitable access to  
610 greenspaces, communicating their multiple benefits, and considering their use to restrict development in hazardous areas will  
611 be key to sustainable, risk-informed urban growth.

#### 612 **Data availability**

613 The data used to support the findings and results of this study are available in the supplementary information and in the  
614 Zenodo repository <https://doi.org/10.5281/zenodo.5881876>. Pleiades imagery data were provided through the CEOS Seismic  
615 Hazard Demonstrator and are restricted by license.

#### 616 **Author contribution**

617 All authors have read and agreed to the published version of the manuscript. CSW, ES, MAV, JRE, and SKE designed the  
618 concept. JRE, CZ, SB-B, PC, DFO provided access to datasets. CSW performed the analysis and prepared the figures. CSW  
619 wrote the manuscript with input from all authors.

#### 620 **Competing interests**

621 The authors declare that they have no conflict of interest.

#### 622 **Financial support**

623 This research has been supported the UK Research and Innovation (UKRI) Global Challenges Research Fund (GCRF) Urban  
624 Disaster Risk Hub (NE/S009000/1) (Tomorrow's Cities), a NERC Innovation award (grant number NE/S013911/1), and  
625 COMET. COMET is the NERC Centre for the Observation and Modelling of Earthquakes, Volcanoes and Tectonics, a  
626 partnership between UK Universities and the British Geological Survey. John Elliott is supported by a Royal Society  
627 University Research fellowship (UF150282) and Susanna Ebmeier is supported by a NERC Independent Research  
628 Fellowship (NE/R015546/1).

#### 629 **Acknowledgments**

630 The Committee on Earth Observation Satellites (CEOS) and Centre National d'Etudes Spatiales (CNES) are thanked for  
631 providing access to the Pleiades satellite imagery used in this study. Pleiades images were made available by CNES in the  
632 framework of the CEOS Working Group for Disasters. © CNES (2018, 2019, 2020), and Airbus DS, all rights reserved.  
633 Commercial uses forbidden.

634 **References**

- 635 Airbus Defence and Space: Pléiades Imagery User Guide. [Accessed 29th October 2019] Available from:  
636 <https://www.intelligence-airbusds.com/en/8718-user-guides>, 2012.
- 637 Allan, P., Bryant, M., Wirsching, C., Garcia, D., and Teresa Rodriguez, M.: The Influence of Urban Morphology on the  
638 Resilience of Cities Following an Earthquake, *Journal of Urban Design*, 18, 242-262, 10.1080/13574809.2013.772881, 2013.
- 639 Altieri, M. A., Companioni, N., Cañizares, K., Murphy, C., Rosset, P., Bourque, M., and Nicholls, C. I.: The greening of the  
640 “barrios”: Urban agriculture for food security in Cuba, *Agriculture and Human Values*, 16, 131-140,  
641 10.1023/A:1007545304561, 1999.
- 642 Alvarado, A., Audin, L., Nocquet, J. M., Lagreulet, S., Segovia, M., Font, Y., Lamarque, G., Yepes, H., Mothes, P.,  
643 Rolandone, F., Jarrín, P., and Quidelleur, X.: Active tectonics in Quito, Ecuador, assessed by geomorphological studies, GPS  
644 data, and crustal seismicity, 33, 67-83, 10.1002/2012tc003224, 2014.
- 645 Amey, R. M. J., Elliott, J. R., Hussain, E., Walker, R., Pagani, M., Silva, V., Abdrakhmatov, K. E., and Watson, C. S.:  
646 Significant Seismic Risk Potential from Buried Faults Beneath Almaty City, Kazakhstan, revealed from high-resolution  
647 satellite DEMs, *Earth and Space Science*, <https://doi.org/10.1029/2021EA001664>, 2021.
- 648 Anhorn, J., and Khazai, B.: Open space suitability analysis for emergency shelter after an earthquake, *Nat. Hazards Earth*  
649 *Syst. Sci.*, 15, 789-803, 10.5194/nhess-15-789-2015, 2015.
- 650 Aragundi, S. M., Mena, A. P., and Zamora, J. J.: Historical Urban Landscape as a Descriptive Feature for Risk Assessment:  
651 the ‘Quebradas’ of Quito, FICUP. An International Conference on Urban Physics, Quito – Galápagos, Ecuador, 2016.
- 652 Aronson, M. F., Lepczyk, C. A., Evans, K. L., Goddard, M. A., Lerman, S. B., MacIvor, J. S., Nilon, C. H., and Vargo, T.:  
653 Biodiversity in the city: key challenges for urban green space management, *Frontiers in Ecology and the Environment*, 15,  
654 189-196, <https://doi.org/10.1002/fee.1480>, 2017.
- 655 Baker, J. L.: *Climate Change, Disaster Risk, and the Urban Poor*, Climate Change, Disaster Risk, and the Urban Poor, 2012.
- 656 Bauwelinck, M., Casas, L., Nawrot, T. S., Nemery, B., Trabelsi, S., Thomas, I., Aerts, R., Lefebvre, W., Vanpoucke, C., Van  
657 Nieuwenhuysse, A., Deboosere, P., and Vandenheede, H.: Residing in urban areas with higher green space is associated with  
658 lower mortality risk: A census-based cohort study with ten years of follow-up, *Environment International*, 148, 106365,  
659 <https://doi.org/10.1016/j.envint.2020.106365>, 2021.
- 660 Beauval, C., Mariniere, J., Yepes, H., Audin, L., Nocquet, J. M., Alvarado, A., Baize, S., Aguilar, J., Singaicho, J., and  
661 Jomard, H.: A New Seismic Hazard Model for Ecuador, *Bulletin of the Seismological Society of America*, 108,  
662 10.1785/0120170259, 2018.
- 663 Benedict, M., and MacMahon, E.: *Green Infrastructure: Smart Conservation for the 21st Century*, 2002.
- 664 Beven, K. J., and Kirkby, M. J.: A physically based, variable contributing area model of basin hydrology / Un modèle à base  
665 physique de zone d'appel variable de l'hydrologie du bassin versant, *Hydrological Sciences Bulletin*, 24, 43-69,  
666 10.1080/02626667909491834, 1979.
- 667 Bonilla-Bedoya, S., Estrella, A., Vaca Yáñez, A., and Herrera, M. Á.: Urban socio-ecological dynamics: applying the urban-  
668 rural gradient approach in a high Andean city, *Landscape Research*, 45, 327-345, 10.1080/01426397.2019.1641589, 2020a.

- 669 Bonilla-Bedoya, S., Mora, A., Vaca, A., Estrella, A., and Herrera, M. Á.: Modelling the relationship between urban  
670 expansion processes and urban forest characteristics: An application to the Metropolitan District of Quito, *Computers,*  
671 *Environment and Urban Systems*, 79, 101420, <https://doi.org/10.1016/j.compenvurbsys.2019.101420>, 2020b.
- 672 Borland, J.: Small parks, big designs: reconstructed Tokyo's new green spaces, 1923–1931, *Urban History*, 47, 106-125,  
673 10.1017/S0963926819000567, 2020.
- 674 Boulton, C., Dedekorkut-Howes, A., and Byrne, J.: Factors shaping urban greenspace provision: A systematic review of the  
675 literature, *Landscape and Urban Planning*, 178, 82-101, <https://doi.org/10.1016/j.landurbplan.2018.05.029>, 2018.
- 676 Bryant, M., and Allan, P.: Open space innovation in earthquake affected cities, in: *Approaches to Disaster Management -*  
677 *Examining the Implications of Hazards, Emergencies and Disasters*, edited by: (ed.), J. P. T., In-Tech, 2013.
- 678 Cardona, O., Aalst, M., Birkmann, J., Fordham, M., McGregor, G., Perez, R., Pulwarty, R., Schipper, L., and Sinh, B.:  
679 Determinants of risk: Exposure and vulnerability, in managing the risks of extreme events and disasters to advance climate  
680 change adaptation, 65-108 pp., 2012.
- 681 Carmin, J., and Anguelovski, I.: *Planning Climate Resilient Cities: Early Lessons from Early Adapters*, 2009.
- 682 Carrión, F., and Erazo Espinosa, J.: La forma urbana de Quito: una historia de centros y periferias, *Bulletin de l'Institut*  
683 *français d'études andines*, 503-522, 2012.
- 684 Castelo, C. A. J., D'Howitt, M. C., Almeida, O. P., and Toulkeridis, T.: Comparative Determination of the Probability of  
685 Landslide Occurrences and Susceptibility in Central Quito, Ecuador, 2018 International Conference on eDemocracy &  
686 eGovernment (ICEDEG), 2018, 136-143,
- 687 Chatelain, J. L., Tucker, B., Guillier, B., Kaneko, F., Yepes, H., Fernandez, J., Valverde, J., Hoefler, G., Souris, M., Dupérier,  
688 E., Yamada, T., Bustamante, G., and Villacis, C.: Earthquake risk management pilot project in Quito, Ecuador, *GeoJournal*,  
689 49, 185-196, 10.1023/A:1007079403225, 1999.
- 690 Colding, J., and Barthel, S.: The potential of 'Urban Green Commons' in the resilience building of cities, *Ecological*  
691 *Economics*, 86, 156-166, <https://doi.org/10.1016/j.ecolecon.2012.10.016>, 2013.
- 692 Cuvi, N., and Vélez, L. C. G.: Los Parques Urbanos de Quito: Distribución, Accesibilidad y Segregación Espacial,  
693 *Environmental Science*, 10, 2021.
- 694 De Sherbinin, A., Schiller, A., and Pulsipher, A.: The vulnerability of global cities to climate hazards, *Environment and*  
695 *Urbanization*, 19, 39-64, 10.1177/0956247807076725, 2007.
- 696 Deng, J., Huang, Y., Chen, B., Tong, C., Liu, P., Wang, H., and Hong, Y.: A Methodology to Monitor Urban Expansion and  
697 Green Space Change Using a Time Series of Multi-Sensor SPOT and Sentinel-2A Images, *Remote Sensing*, 11, 1230, 2019.
- 698 DMQ: *Visión de Quito 2040 y su Nuevo Modelo de Ciudad*, 2018.
- 699 Domínguez-Castro, F., García-Herrera, R., and Vicente-Serrano, S. M.: Wet and dry extremes in Quito (Ecuador) since the  
700 17th century, *International Journal of Climatology*, 38, 2006-2014, 10.1002/joc.5312, 2018.
- 701 Dou, K., and Zhan, Q.: Accessibility analysis of urban emergency shelters: Comparing gravity model and space syntax, 2011  
702 International Conference on Remote Sensing, Environment and Transportation Engineering, 2011, 5681-5684,



- 703 Emberson, R., Kirschbaum, D., and Stanley, T.: New global characterisation of landslide exposure, *Nat. Hazards Earth Syst. Sci.*, 20, 3413-3424, 10.5194/nhess-20-3413-2020, 2020.
- 704
- 705 Escobedo, F. J., and Nowak, D. J.: Spatial heterogeneity and air pollution removal by an urban forest, *Landscape and Urban Planning*, 90, 102-110, <https://doi.org/10.1016/j.landurbplan.2008.10.021>, 2009.
- 706
- 707 Estrella, M., and Saalimaa, N.: Ecosystem-based disaster risk reduction (Eco-DRR): An overview, *The role of ecosystems in disaster risk reduction*, edited by: Renaud, F. G., Sudmeier-Rieux, K., and Estrella, M., United Nations University Press, 2013.
- 708
- 709
- 710 Faivre, N., Sgobbi, A., Happaerts, S., Raynal, J., and Schmidt, L.: Translating the Sendai Framework into action: The EU approach to ecosystem-based disaster risk reduction, *International Journal of Disaster Risk Reduction*, 32, 4-10, <https://doi.org/10.1016/j.ijdr.2017.12.015>, 2018.
- 711
- 712
- 713 Farr, T. G., Rosen, P. A., Caro, E., Crippen, R., Duren, R., Hensley, S., Kobrick, M., Paller, M., Rodriguez, E., Roth, L., Seal, D., Shaffer, S., Shimada, J., Umland, J., Werner, M., Oskin, M., Burbank, D., and Alsdorf, D.: The Shuttle Radar Topography Mission, *Reviews of Geophysics*, 45, 10.1029/2005RG000183, 2007.
- 714
- 715
- 716 Fenger, J.: Urban air quality, *Atmospheric Environment*, 33, 4877-4900, [https://doi.org/10.1016/S1352-2310\(99\)00290-3](https://doi.org/10.1016/S1352-2310(99)00290-3), 1999.
- 717
- 718 Flörke, M., Schneider, C., and McDonald, R. I.: Water competition between cities and agriculture driven by climate change and urban growth, *Nature Sustainability*, 1, 51-58, 10.1038/s41893-017-0006-8, 2018.
- 719
- 720 Froude, M. J., and Petley, D. N.: Global fatal landslide occurrence from 2004 to 2016, *Nat. Hazards Earth Syst. Sci.*, 18, 2161-2181, 10.5194/nhess-18-2161-2018, 2018.
- 721
- 722 Fuller, R., Groom, G., and Jones, A.: The land-cover map of great Britain: an automated classification of landsat thematic mapper data, *Photogrammetric Engineering and Remote Sensing*, 60, 553-562, 1994.
- 723
- 724 Galasso, C., McCloskey, J., Pelling, M., Hope, M., Bean, C. J., Cremen, G., Guragain, R., Hancilar, U., Menoscal, J., Mwang'a, K., Phillips, J., Rush, D., and Sinclair, H.: Editorial. Risk-based, Pro-poor Urban Design and Planning for Tomorrow's Cities, *International Journal of Disaster Risk Reduction*, 58, 102158, <https://doi.org/10.1016/j.ijdr.2021.102158>, 2021.
- 725
- 726
- 727
- 728 García-Lamarca, M., Connolly, J., and Anguelovski, I.: Green gentrification and displacement in Barcelona, in: *Housing Displacement*, Routledge, 156-170, 2020.
- 729
- 730 Georganos, S., Grippa, T., Vanhuysse, S., Lennert, M., Shimoni, M., and Wolff, E.: Very High Resolution Object-Based Land Use–Land Cover Urban Classification Using Extreme Gradient Boosting, *IEEE Geoscience and Remote Sensing Letters*, 15, 607-611, 10.1109/LGRS.2018.2803259, 2018.
- 731
- 732
- 733 Gill, J. C., and Malamud, B. D.: Anthropogenic processes, natural hazards, and interactions in a multi-hazard framework, *Earth-Science Reviews*, 166, 246-269, <https://doi.org/10.1016/j.earscirev.2017.01.002>, 2017.
- 734
- 735 Gill, J. C., Hussain, E., and Malamud, B. D.: Workshop Report: Multi-Hazard Risk Scenarios for Tomorrow's Cities. [Accessed 18th May 2021]. Available from: <https://tomorrowscities.org/workshop-report-multi-hazard-risk-scenarios-tomorrows-cities>, 2021.
- 736
- 737

- 738 Godfray, H. C. J., Beddington, J. R., Crute, I. R., Haddad, L., Lawrence, D., Muir, J. F., Pretty, J., Robinson, S., Thomas, S.  
739 M., and Toulmin, C.: Food Security: The Challenge of Feeding 9 Billion People, *Science*, 327, 812-818,  
740 10.1126/science.1185383, 2010.
- 741 Gonzalez, C. G.: Seasons of Resistance: Sustainable Agriculture and Food Security in Cuba, *Tulane Environmental Law*  
742 *Journal*, 16, 685-732, 2003.
- 743 Gorelick, N., Hancher, M., Dixon, M., Ilyushchenko, S., Thau, D., and Moore, R.: Google Earth Engine: Planetary-scale  
744 geospatial analysis for everyone, *Remote Sensing of Environment*, 202, 18-27, <https://doi.org/10.1016/j.rse.2017.06.031>,  
745 2017.
- 746 Gregory McPherson, E.: Accounting for benefits and costs of urban greenspace, *Landscape and Urban Planning*, 22, 41-51,  
747 [https://doi.org/10.1016/0169-2046\(92\)90006-L](https://doi.org/10.1016/0169-2046(92)90006-L), 1992.
- 748 Hall, M. L., Samaniego, P., Le Pennec, J. L., and Johnson, J. B.: Ecuadorian Andes volcanism: A review of Late Pliocene to  
749 present activity, *Journal of Volcanology and Geothermal Research*, 176, 1-6,  
750 <https://doi.org/10.1016/j.jvolgeores.2008.06.012>, 2008.
- 751 Hastenrath, S.: Annual cycle of upper air circulation and convective activity over the tropical Americas, *Journal of*  
752 *Geophysical Research: Atmospheres*, 102, 4267-4274, <https://doi.org/10.1029/96JD03122>, 1997.
- 753 Hoekstra, A. Y., Buurman, J., and van Ginkel, K. C. H.: Urban water security: A review, *Environ. Res. Lett.*, 13, 053002,  
754 10.1088/1748-9326/aaba52, 2018.
- 755 Hosseini, S. A., de la Fuente, A., and Pons, O.: Multicriteria decision-making method for sustainable site location of post-  
756 disaster temporary housing in urban areas, *Journal of Construction Engineering and Management*, 142, 04016036, 2016.
- 757 IG-EPN, IGM, IRD.: Mapa de Peligros Volcánicos Potenciales del Volcán Guagua Pichincha 3ra. Edición, Quito - Ecuador.  
758 Available online: <https://www.igepep.edu.ec/ggp-mapa-de-peligros/file> (accessed 10 December 2020). 2019.
- 759 Inglada, J., and Christophe, E.: The Orfeo Toolbox remote sensing image processing software, 2009 IEEE International  
760 Geoscience and Remote Sensing Symposium, 2009, IV-733-IV-736,
- 761 Instituto Geográfico Militar: Fotografía aérea 360 Rollo 19 Cámara RC10 Proyecto Carta Nacional N-III\_1977 Escala  
762 1:60000 B/N. [online]. Accessed: 20 March 2020. Available from:  
763 <http://www.geoportalmgm.gob.ec/geonetwork/srv/spa/catalog.search#/metadata/e56534b0-3b16-423e-a076-e0e41df07a81>,  
764 1977.
- 765 Instituto Geográfico Militar: Generation of geospatial information at a scale 1: 5 000 for the determination of the physical  
766 fitness of the territory and urban development through the use of geotechnologies [Spanish], 2019.
- 767 Jalayer, F., De Risi, R., De Paola, F., Giugni, M., Manfredi, G., Gasparini, P., Topa, M. E., Yonas, N., Yeshitela, K.,  
768 Nebebe, A., Cavan, G., Lindley, S., Printz, A., and Renner, F.: Probabilistic GIS-based method for delineation of urban  
769 flooding risk hotspots, *Natural Hazards*, 73, 975-1001, 10.1007/s11069-014-1119-2, 2014.
- 770 James, P., Banay, R. F., Hart, J. E., and Laden, F.: A Review of the Health Benefits of Greenness, *Current Epidemiology*  
771 *Reports*, 2, 131-142, 10.1007/s40471-015-0043-7, 2015.

- 772 Jeong, D., Kim, M., Song, K., and Lee, J.: Planning a Green Infrastructure Network to Integrate Potential Evacuation Routes  
773 and the Urban Green Space in a Coastal City: The Case Study of Haeundae District, Busan, South Korea, *Science of The*  
774 *Total Environment*, 761, 143179, <https://doi.org/10.1016/j.scitotenv.2020.143179>, 2021.
- 775 Kelleher, C., and McPhillips, L.: Exploring the application of topographic indices in urban areas as indicators of pluvial  
776 flooding locations, *Hydrological Processes*, 34, 780-794, 2020.
- 777 Kennedy, R. E., Yang, Z., Gorelick, N., Braaten, J., Cavalcante, L., Cohen, W. B., and Healey, S.: Implementation of the  
778 LandTrendr Algorithm on Google Earth Engine, *Remote Sensing*, 10, 691, 2018.
- 779 Khazai, B., Anhorn, J., Girard, T., Brink, S., Daniell, J., Bessel, T., Mühr, B., Flörchinger, V., and Kunz-Plapp, T.: Shelter  
780 response and vulnerability of displaced populations in the April 25, 2015 Nepal Earthquake, Center for Disaster  
781 Management and Risk Reduction Technology of the Karlsruhe Institute of Technology, and the South Asia Institute,  
782 Heidelberg University, 5, 2015, 2015.
- 783 Kılçı, F., Kara, B. Y., and Bozkaya, B.: Locating temporary shelter areas after an earthquake: A case for Turkey, *European*  
784 *Journal of Operational Research*, 243, 323-332, <https://doi.org/10.1016/j.ejor.2014.11.035>, 2015.
- 785 Kirschbaum, D., Stanley, T., and Yatheendradas, S.: Modeling landslide susceptibility over large regions with fuzzy overlay,  
786 *Landslides*, 13, 485-496, 10.1007/s10346-015-0577-2, 2016.
- 787 Kirschbaum, D., and Stanley, T.: Satellite-Based Assessment of Rainfall-Triggered Landslide Hazard for Situational  
788 Awareness, *Earth's Future*, 6, <https://doi.org/doi:10.1002/2017EF000715>, 2018.
- 789 Kumar, P., Debele, S. E., Sahani, J., Rawat, N., Marti-Cardona, B., Alfieri, S. M., Basu, B., Basu, A. S., Bowyer, P.,  
790 Charizopoulos, N., Jaakko, J., Loupis, M., Menenti, M., Mickovski, S. B., Pfeiffer, J., Pilla, F., Pröll, J., Pulvirenti, B.,  
791 Rutzinger, M., Sannigrahi, S., Spyrou, C., Tuomenvirta, H., Vojinovic, Z., and Zieher, T.: An overview of monitoring  
792 methods for assessing the performance of nature-based solutions against natural hazards, *Earth-Science Reviews*, 217,  
793 103603, <https://doi.org/10.1016/j.earscirev.2021.103603>, 2021.
- 794 Labib, S. M., and Harris, A.: The potentials of Sentinel-2 and LandSat-8 data in green infrastructure extraction, using object  
795 based image analysis (OBIA) method, *European Journal of Remote Sensing*, 51, 231-240, 10.1080/22797254.2017.1419441,  
796 2018.
- 797 Leblon, B., Gallant, L., and Granberg, H.: Effects of shadowing types on ground-measured visible and near-infrared shadow  
798 reflectances, *Remote Sensing of Environment*, 58, 322-328, [https://doi.org/10.1016/S0034-4257\(96\)00079-X](https://doi.org/10.1016/S0034-4257(96)00079-X), 1996.
- 799 Lidberg, W., Nilsson, M., Lundmark, T., and Ågren, A. M.: Evaluating preprocessing methods of digital elevation models  
800 for hydrological modelling, *Hydrological Processes*, 31, 4660-4668, 2017.
- 801 Liu, Q., Ruan, X., and Shi, P.: Selection of emergency shelter sites for seismic disasters in mountainous regions: Lessons  
802 from the 2008 Wenchuan Ms 8.0 Earthquake, China, *Journal of Asian Earth Sciences*, 40, 926-934, 2011.
- 803 Loughlin, S. C., Sparks, R. S. J., Sparks, S., Brown, S. K., Jenkins, S. F., and Vye-Brown, C.: Global volcanic hazards and  
804 risk, Cambridge University Press, 2015.
- 805 Manfreda, S., Di Leo, M., and Sole, A.: Detection of flood-prone areas using digital elevation models, *Journal of Hydrologic*  
806 *Engineering*, 16, 781-790, 2011.

- 807 Maragno, D., Gaglio, M., Robbi, M., Appiotti, F., Fano, E. A., and Gissi, E.: Fine-scale analysis of urban flooding reduction  
808 from green infrastructure: An ecosystem services approach for the management of water flows, *Ecological Modelling*, 386,  
809 1-10, <https://doi.org/10.1016/j.ecolmodel.2018.08.002>, 2018.
- 810 Markus, T., Neumann, T., Martino, A., Abdalati, W., Brunt, K., Csatho, B., Farrell, S., Fricker, H., Gardner, A., Harding, D.,  
811 Jasinski, M., Kwok, R., Magruder, L., Lubin, D., Luthcke, S., Morison, J., Nelson, R., Neuenschwander, A., Palm, S.,  
812 Popescu, S., Shum, C. K., Schutz, B. E., Smith, B., Yang, Y., and Zwally, J.: The Ice, Cloud, and land Elevation Satellite-2  
813 (ICESat-2): Science requirements, concept, and implementation, *Remote Sensing of Environment*, 190, 260-273,  
814 <https://doi.org/10.1016/j.rse.2016.12.029>, 2017.
- 815 Marmot, M., Friel, S., Bell, R., Houweling, T. A. J., and Taylor, S.: Closing the gap in a generation: health equity through  
816 action on the social determinants of health, *The Lancet*, 372, 1661-1669, [https://doi.org/10.1016/S0140-6736\(08\)61690-6](https://doi.org/10.1016/S0140-6736(08)61690-6),  
817 2008.
- 818 Marselle, M. R., Bowler, D. E., Watzema, J., Eichenberg, D., Kirsten, T., and Bonn, A.: Urban street tree biodiversity and  
819 antidepressant prescriptions, *Scientific Reports*, 10, 22445, 10.1038/s41598-020-79924-5, 2020.
- 820 Mattivi, P., Franci, F., Lambertini, A., and Bitelli, G.: TWI computation: a comparison of different open source GISs, *Open*  
821 *Geospatial Data, Software and Standards*, 4, 1-12, 2019.
- 822 McDonald, R. I., Mansur, A. V., Ascensão, F., Colbert, M. I., Crossman, K., Elmqvist, T., Gonzalez, A., Güneralp, B.,  
823 Haase, D., Hamann, M., Hillel, O., Huang, K., Kahnt, B., Maddox, D., Pacheco, A., Pereira, H. M., Seto, K. C., Simkin, R.,  
824 Walsh, B., Werner, A. S., and Ziter, C.: Research gaps in knowledge of the impact of urban growth on biodiversity, *Nature*  
825 *Sustainability*, 3, 16-24, 10.1038/s41893-019-0436-6, 2020.
- 826 McVittie, A., Cole, L., Wreford, A., Sgobbi, A., and Yordi, B.: Ecosystem-based solutions for disaster risk reduction:  
827 Lessons from European applications of ecosystem-based adaptation measures, *International Journal of Disaster Risk*  
828 *Reduction*, 32, 42-54, <https://doi.org/10.1016/j.ijdr.2017.12.014>, 2018.
- 829 Metro Ecuador: En caso de un sismo en Quito, estos son los sitios seguros en la ciudad. Metro Ecuador. [Online]. 12  
830 December. [Accessed 01 November 2021]. Available from: [https://www.metroecuador.com.ec/ec/noticias/2019/05/28/caso-](https://www.metroecuador.com.ec/ec/noticias/2019/05/28/caso-temblor-estos-los-sitios-seguros-quito.html)  
831 [temblor-estos-los-sitios-seguros-quito.html](https://www.metroecuador.com.ec/ec/noticias/2019/05/28/caso-temblor-estos-los-sitios-seguros-quito.html). 2019.
- 832 Millard, K., and Richardson, M.: On the Importance of Training Data Sample Selection in Random Forest Image  
833 Classification: A Case Study in Peatland Ecosystem Mapping, *Remote. Sens.*, 7, 8489-8515, 2015.
- 834 Ministry of Territory. Habitat and Housing.: Accidentes.  
835 <https://territorio.maps.arcgis.com/home/item.html?id=5270bc85cf3249b29937d25d0b363396>, 2020.
- 836 Myint, S. W., Gober, P., Brazel, A., Grossman-Clarke, S., and Weng, Q.: Per-pixel vs. object-based classification of urban  
837 land cover extraction using high spatial resolution imagery, *Remote Sensing of Environment*, 115, 1145-1161,  
838 <http://dx.doi.org/10.1016/j.rse.2010.12.017>, 2011.
- 839 Neumann, T. A., Martino, A. J., Markus, T., Bae, S., Bock, M. R., Brenner, A. C., Brunt, K. M., Cavanaugh, J., Fernandes,  
840 S. T., Hancock, D. W., Harbeck, K., Lee, J., Kurtz, N. T., Luers, P. J., Luthcke, S. B., Magruder, L., Pennington, T. A.,  
841 Ramos-Izquierdo, L., Rebold, T., Skoog, J., and Thomas, T. C.: The Ice, Cloud, and Land Elevation Satellite – 2 mission: A  
842 global geolocated photon product derived from the Advanced Topographic Laser Altimeter System, *Remote Sensing of*  
843 *Environment*, 233, 111325, <https://doi.org/10.1016/j.rse.2019.111325>, 2019.

- 844 Neumann, T. A., Brenner, A., Hancock, D., Robbins, J., Saba, J., Harbeck, K., Gibbons, A., Lee, J., Luthcke, S. B., and  
845 Rebold, T.: ATLAS/ICESat-2 L2A Global Geolocated Photon Data, Version 3. Boulder, Colorado USA. NASA National  
846 Snow and Ice Data Center Distributed Active Archive Center. doi: <https://doi.org/10.5067/ATLAS/ATL03.003>. [Accessed  
847 7th December 2020]. 2020.
- 848 Nuth, C., and Kääb, A.: Co-registration and bias corrections of satellite elevation data sets for quantifying glacier thickness  
849 change, *The Cryosphere*, 5, 271-290, <https://doi.org/10.1016/10.5194/tc-5-271-2011>, 2011.
- 850 Oliver-Smith, A., Alcántara-Ayala, I., I. B., and Lavell, A.: Forensic Investigations of Disasters (FORIN): a conceptual  
851 framework and guide to research. Available online: [http://www.irdrinternational.org/wp-content/uploads/2016/01/FORIN-2-](http://www.irdrinternational.org/wp-content/uploads/2016/01/FORIN-2-29022016.pdf)  
852 [29022016.pdf](http://www.irdrinternational.org/wp-content/uploads/2016/01/FORIN-2-29022016.pdf)  
853 (accessed on 11 November 2019). 2016.
- 854 Olofsson, P., Foody, G. M., Stehman, S. V., and Woodcock, C. E.: Making better use of accuracy data in land change  
855 studies: Estimating accuracy and area and quantifying uncertainty using stratified estimation, *Remote Sensing of*  
856 *Environment*, 129, 122-131, <https://doi.org/10.1016/j.rse.2012.10.031>, 2013.
- 857 Olofsson, P., Foody, G. M., Herold, M., Stehman, S. V., Woodcock, C. E., and Wulder, M. A.: Good practices for estimating  
858 area and assessing accuracy of land change, *Remote Sensing of Environment*, 148, 42-57,  
859 <https://doi.org/10.1016/j.rse.2014.02.015>, 2014.
- 860 Onuma, A., and Tsuge, T.: Comparing green infrastructure as ecosystem-based disaster risk reduction with gray  
861 infrastructure in terms of costs and benefits under uncertainty: A theoretical approach, *International Journal of Disaster Risk*  
862 *Reduction*, 32, 22-28, <https://doi.org/10.1016/j.ijdr.2018.01.025>, 2018.
- 863 Pagani, M., Garcia-Pelaez, J., Gee, R., Johnson, K., Poggi, V., Styron, R., Weatherill, G., Simionato, M., Viganò, D.,  
864 Danciu, L., and Monelli, D.: Global Earthquake Model (GEM) Seismic Hazard Map (version 2018.1 - December 2018).  
865 Available online: <https://www.globalquakemodel.org/gem-maps/global-earthquake-hazard-map> (accessed 5 May 2021).  
866 DOI: 10.13117/GEM-GLOBAL-SEISMIC-HAZARD-MAP-2018.1, 2018.
- 867 Passalacqua, P., Belmont, P., Staley, D. M., Simley, J. D., Arrowsmith, J. R., Bode, C. A., Crosby, C., DeLong, S. B., Glenn,  
868 N. F., Kelly, S. A., Lague, D., Sangireddy, H., Schaffrath, K., Tarboton, D. G., Wasklewicz, T., and Wheaton, J. M.:  
869 Analyzing high resolution topography for advancing the understanding of mass and energy transfer through landscapes: A  
870 review, *Earth-Science Reviews*, 148, 174-193, <http://dx.doi.org/10.1016/j.earscirev.2015.05.012>, 2015.
- 871 Pelling, M., Maskrey, A., Ruiz, P., Hall, P., Peduzzi, P., Dao, Q.-H., Mouton, F., Herold, C., and Kluser, S.: Reducing  
872 disaster risk: a challenge for development, 2004.
- 873 Peralta Arias, J. J., and Higuera García, E.: Evaluación sostenible de los Planes Directores de Quito. Periodo 1942-2012,  
874 2016.
- 875 Perrin, J. L., Bouvier, C., Janeau, J. L., Ménez, G., and Cruz, F.: Rainfall/runoff processes in a small peri-urban catchment in  
876 the Andes mountains. The Rumihurcu Quebrada, Quito (Ecuador), *Hydrological Processes*, 15, 843-854,  
877 <https://doi.org/10.1002/hyp.190>, 2001.
- 878 Pettorelli, N., Vik, J. O., Mysterud, A., Gaillard, J.-M., Tucker, C. J., and Stenseth, N. C.: Using the satellite-derived NDVI  
879 to assess ecological responses to environmental change, *Trends in Ecology & Evolution*, 20, 503-510,  
880 <https://doi.org/10.1016/j.tree.2005.05.011>, 2005.

- 881 Phillips, C., and Marden, M.: Reforestation Schemes to Manage Regional Landslide Risk, in: *Landslide Hazard and Risk*,  
882 517-547, 2005.
- 883 Rebotier, J.: *El riesgo y su gestión en Ecuador: una mirada de geografía social y política*, Centro de Publicaciones Pontificia  
884 Universidad Católica del Ecuador, 2016.
- 885 Robin, C., Samaniego, P., Le Pennec, J.-L., Mothes, P., and van der Plicht, J.: Late Holocene phases of dome growth and  
886 Plinian activity at Guagua Pichincha volcano (Ecuador), *Journal of Volcanology and Geothermal Research*, 176, 7-15,  
887 <https://doi.org/10.1016/j.jvolgeores.2007.10.008>, 2008.
- 888 Rodriguez-Galiano, V. F., Ghimire, B., Rogan, J., Chica-Olmo, M., and Rigol-Sanchez, J. P.: An assessment of the  
889 effectiveness of a random forest classifier for land-cover classification, *ISPRS Journal of Photogrammetry and Remote  
890 Sensing*, 67, 93-104, <https://doi.org/10.1016/j.isprsjprs.2011.11.002>, 2012.
- 891 Salazar, E., Henríquez, C., Sliuzas, R., and Qüense, J.: Evaluating Spatial Scenarios for Sustainable Development in Quito,  
892 Ecuador, *ISPRS Int. J. Geo Inf.*, 9, 141, 2020.
- 893 Salazar, E., Henríquez, C., Durán, G., Qüense, J., and Puente-Sotomayor, F.: How to Define a New Metropolitan Area? The  
894 Case of Quito, Ecuador, and Contributions for Urban Planning, *Land*, 10, 413, 2021.
- 895 Salmon, N., Yépez, G., Duque, M., Yépez, M., Báez, A., Masache-Heredia, M., Mejía, G., Mejía, P., Garofalo, G., and  
896 Montoya, D.: Co-design of a Nature-Based Solutions Ecosystem for Reactivating a Peri-Urban District in Quito, Ecuador, in:  
897 *Governance of Climate Responsive Cities: Exploring Cross-Scale Dynamics*, edited by: Peker, E., and Ataöv, A., Springer  
898 International Publishing, Cham, 79-104, 2021.
- 899 Sandholz, S., Lange, W., and Nehren, U.: Governing green change: Ecosystem-based measures for reducing landslide risk in  
900 Rio de Janeiro, *International Journal of Disaster Risk Reduction*, 32, 75-86, <https://doi.org/10.1016/j.ijdrr.2018.01.020>, 2018.
- 901 Schneider, A., and Woodcock, C. E.: Compact, Dispersed, Fragmented, Extensive? A Comparison of Urban Growth in  
902 Twenty-five Global Cities using Remotely Sensed Data, Pattern Metrics and Census Information, *Urban Studies*, 45, 659-  
903 692, 10.1177/0042098007087340, 2008.
- 904 Shimpó, N., Wesener, A., and McWilliam, W.: How community gardens may contribute to community resilience following  
905 an earthquake, *Urban Forestry & Urban Greening*, 38, 124-132, <https://doi.org/10.1016/j.ufug.2018.12.002>, 2019.
- 906 Shrestha, S. R., Sliuzas, R., and Kuffer, M.: Open spaces and risk perception in post-earthquake Kathmandu city, *Applied  
907 Geography*, 93, 81-91, <https://doi.org/10.1016/j.apgeog.2018.02.016>, 2018.
- 908 Sierra, A.: *La política de mitigación de los riesgos en las laderas de Quito: ¿qué vulnerabilidad combatir?*, 2009,
- 909 SNI: *Archivos de Informacion Geografica. Peligro Volcánico* [Accessed 24 August 2020], 2020.
- 910 Sphere Association: *The Sphere Handbook: Humanitarian Charter and Minimum Standards in Humanitarian Response*,  
911 fourth edition, Geneva, Switzerland,  
912 [www.spherestandards.org/handbook](http://www.spherestandards.org/handbook), 2018.
- 913 Stanley, T., and Kirschbaum, D. B.: A heuristic approach to global landslide susceptibility mapping, *Natural Hazards*, 87,  
914 145-164, <https://doi.org/10.1007/s11069-017-2757-y>, 2017.

- 915 Styron, R.: GEMScienceTools/gem-global-active-faults: First release of 2019 (Version 2019.0), ZENODO,  
916 <http://doi.org/10.5281/zenodo.3376300>, 2019.
- 917 Sudmeier-Rieux, K., Arce-Mojica, T., Boehmer, H. J., Doswald, N., Emerton, L., Friess, D. A., Galvin, S., Hagenlocher, M.,  
918 James, H., Laban, P., Lacambra, C., Lange, W., McAdoo, B. G., Moos, C., Mysiak, J., Narvaez, L., Nehren, U., Peduzzi, P.,  
919 Renaud, F. G., Sandholz, S., Schreyers, L., Sebesvari, Z., Tom, T., Triyanti, A., van Eijk, P., van Staveren, M., Vicarelli, M.,  
920 and Walz, Y.: Scientific evidence for ecosystem-based disaster risk reduction, *Nature Sustainability*, 4, 803-810,  
921 10.1038/s41893-021-00732-4, 2021.
- 922 Taylor, L., and Hochuli, D. F.: Defining greenspace: Multiple uses across multiple disciplines, *Landscape and Urban  
923 Planning*, 158, 25-38, <https://doi.org/10.1016/j.landurbplan.2016.09.024>, 2017.
- 924 Testori, G.: *Gobierno Barrial de Atucucho. An urban alternative based on self-governance and direct democracy*, 2016.
- 925 Tidball, K. G., and Krasny, M. E.: *Greening in the red zone: Disaster, Resilience and Community Greening*, Springer, 2012.
- 926 Tucker, C. J., Holben, B. N., Elgin, J. H., and McMurtrey, J. E.: Remote sensing of total dry-matter accumulation in winter  
927 wheat, *Remote Sensing of Environment*, 11, 171-189, [https://doi.org/10.1016/0034-4257\(81\)90018-3](https://doi.org/10.1016/0034-4257(81)90018-3), 1981.
- 928 UN-Habitat: *The Challenge of Slums: Global Report on Human Settlements 2003*. Available online:  
929 <https://www.alnap.org/help-library/the-challenge-of-slums-global-report-on-human-settlements-2003> (accessed on 4 May  
930 2021), 2003.
- 931 UN DESA: *World Urbanization Prospects: The 2018 Revision (ST/ESA/SER.A/420)*. New York: United Nations., 2019.
- 932 UN General Assembly: *Transforming our world: the 2030 Agenda for Sustainable Development*. Report No. A/RES/70/1,,  
933 2015.
- 934 Sendai framework for disaster risk reduction 2015 - 2030.:  
935 [https://www.preventionweb.net/files/43291\\_sendaiframeworkfordrren.pdf](https://www.preventionweb.net/files/43291_sendaiframeworkfordrren.pdf), access: 05 February 2020, 2015.
- 936 UNDRR: *Ecosystem-Based Disaster Risk Reduction: Implementing Nature-based Solutions for Resilience*, United Nations  
937 Office for Disaster Risk Reduction – Regional Office for Asia and the Pacific, Bangkok, Thailand, 2020.
- 938 Valcárcel, J., Despotaki, V., Burton, C., Yepes-Estrada, C., Silva, V., and Villacis, C.: *Integrated Assessment of Earthquake  
939 Risk in Quito, Ecuador Using Openquake*, 16th World Conference on Earthquake Engineering, 16WCEE 2017, 2017,
- 940 Valencia, V. H., Levin, G., and Hansen, H. S.: *Modelling the spatial extent of urban growth using a cellular automata-based  
941 model: a case study for Quito, Ecuador*, *Geografisk Tidsskrift-Danish Journal of Geography*, 120, 156-173,  
942 10.1080/00167223.2020.1823867, 2020.
- 943 Vidal, X., Burgos, L., and Zevallos, O.: *11 Protection and environmental restoration of the slopes of Pichincha in Quito,  
944 Ecuador*, *Water and Cities in Latin America: Challenges for Sustainable Development*, 181, 2015.
- 945 Vincenti, S. S., Zuleta, D., Moscoso, V., Jácome, P., Palacios, E., and Villacís, M.: *Análisis estadístico de datos  
946 meteorológicos mensuales y diarios para la determinación de variabilidad climática y cambio climático en el Distrito  
947 Metropolitano de Quito*, *La Granja*, 16, 23-47, 2012.
- 948 WHO Regional Office for Europe: *Urban green spaces and health.*, 2016.

- 949 Wilson, T. M., Stewart, C., Sword-Daniels, V., Leonard, G. S., Johnston, D. M., Cole, J. W., Wardman, J., Wilson, G., and  
950 Barnard, S. T.: Volcanic ash impacts on critical infrastructure, *Physics and Chemistry of the Earth, Parts A/B/C*, 45-46, 5-23,  
951 <https://doi.org/10.1016/j.pce.2011.06.006>, 2012.
- 952 Wolch, J. R., Byrne, J., and Newell, J. P.: Urban green space, public health, and environmental justice: The challenge of  
953 making cities ‘just green enough’, *Landscape and Urban Planning*, 125, 234-244,  
954 <https://doi.org/10.1016/j.landurbplan.2014.01.017>, 2014.
- 955 Yamazaki, F., Liu, W., and Takasaki, M.: Characteristics of shadow and removal of its effects for remote sensing imagery,  
956 2009 IEEE International Geoscience and Remote Sensing Symposium, 4, <https://doi.org/10.1109/IGARSS.2009.5417404>,  
957 2009.
- 958 Zalakeviciute, R., López-Villada, J., and Rybarczyk, Y.: Contrasted Effects of Relative Humidity and Precipitation on Urban  
959 PM2.5 Pollution in High Elevation Urban Areas, *Sustainability*, 10, 2064, 2018.
- 960 Zambrano-Barragán, C., Zevallos, O., Villacís, M., and Enríquez, D.: Quito’s Climate Change Strategy: A Response to  
961 Climate Change in the Metropolitan District of Quito, Ecuador, in: *Resilient Cities*, Dordrecht, 2011, 515-529,
- 962 Zhou, Y., Parsons, B., Elliott, J. R., Barisin, I., and Walker, R. T.: Assessing the ability of Pleiades stereo imagery to  
963 determine height changes in earthquakes: A case study for the El Mayor-Cucapah epicentral area, *Journal of Geophysical*  
964 *Research: Solid Earth*, 120, 8793-8808, 10.1002/2015jb012358, 2015.
- 965 Zhu, Z., Gallant, A. L., Woodcock, C. E., Pengra, B., Olofsson, P., Loveland, T. R., Jin, S., Dahal, D., Yang, L., and Auch,  
966 R. F.: Optimizing selection of training and auxiliary data for operational land cover classification for the LCMAP initiative,  
967 *ISPRS Journal of Photogrammetry and Remote Sensing*, 122, 206-221, <https://doi.org/10.1016/j.isprsjprs.2016.11.004>, 2016.  
968